POLITECNICO DI MILANO

School of Industrial and Information Engineering

Master of Science in Automation and Control Engineering

Goal-driven variable admittance control for robot manual guidance

Supervisor: Prof. Paolo Rocco
Co-supervisor: Ing. Davide Bazzi
Prof. Andrea Maria Zanchettin

Master Thesis dissertation of:

Miriam Lapertosa Id. 899984

Accademic year 2018-2019

"Happiness can be found, even in the darkest of times, if one only remembers to turn on the light."

"You think the dead we loved truly ever leave us? You think we don't recall them more clearly in times of great trouble?"

Albus Percival Wulfric Brian Dumbledore

Ringraziamenti

Ringrazio il Prof. Paolo Rocco per avermi dato l'opportunità di svolgere questa tesi, per la sua disponibilità e per i preziosi consigli.

Ringrazio l'Ing. Davide Bazzi per l'infinita pazienza dimostrata nel corso di questi mesi nei miei confronti. La passione e l'instancabile curiosità con cui svolgi il tuo lavoro sono stati d'ispirazione per me.

Grazie all'Ing. Renzo Villa per i consigli dispensati e per il fondamentale aiuto fornito durante lo svolgimento delle prove sperimentali.

Ringrazio mia madre, Teresa, e mio padre, Vincenzo, sempre presenti in ogni momento, pronti a festeggiare per i miei piccoli successi e a tirarmi su nei momenti difficili. Grazie per i vostri sacrifici, per tutti i "no" che vi siete detti in questi anni per poter dare a me la possibilità di dire qualche "sì" in più. Mi fate sentire fortunata ogni giorno.

Grazie a Francesco, per tutto quello che mi porto dentro, che noi sappiamo, perché "penso che il tempo che ho passato con te, ha cambiato per sempre ogni parte di me". Conosci un altro modo per fregar la morte?

Grazie a Domenico e Mariella, la mia seconda famiglia. Sempre con la parola giusta al momento giusto, in grado di darmi una spinta quando neanche io ci credevo. Il bene che mi avete dato non lo scorderò mai.

Alle amiche di sempre, Eleonora e Noemi. A voi che siete rimaste al mio fianco per tutti questi anni, prendendovi il bello e soprattutto il brutto. A voi che conoscete il mio pessimismo cosmico, le mie paure, i miei dubbi esistenziali ma anche i miei sorrisi più veri. A voi va un ringraziamento che viene dal più profondo del mio cuore.

Grazie a Co, agli audio infiniti che ti sei sorbito senza mai lamentarti. Sei riuscito a vedere in me il meglio, fin dal principio. Mi hai teso una mano e mi hai tirata su in più di un'occasione: non potrò mai ringraziarti abbastanza.

Un ringraziamento speciale a Zu, il miglior ascoltatore che abbia mai avuto la fortuna di incontrare. Grazie per le ore passate a parlare affianco alla fermata della 90. Quante ne abbiamo fatte passare prima che salissi a bordo?

Grazie ad Ale e a Longo, potete mentire quanto volete ma so che mi volete bene (e anche tanto).

Grazie a Dani, Maria, Fabio, Mauri e Gabu per tutte le risate e le ore passate assiame che forse non sono state abbastanza.

Tutti voi siete la famiglia che ho scelto e che, per fortuna, mi ha scelta. Non avrei potuto desiderare dei compagni di viaggio migliori. Vi voglio un bene dell'anima.

Grazie a Raffaele, la mia fotocopia con la barba: sei lo specchio che ogni giorno mi mostra le mie forze e le mie debolezze. Grazie per essermi stato accanto in questi lunghi mesi, condividendo le mie innumerevoli (spesso insensate) ansie e preoccupazioni. Grazie per i consigli, anche per quelli scontati che tanto odio. Infine, ti ringrazio per quelle volte in cui riesci a non farmi pensare a "cosa è giusto e cosa sta cambiando". Il Politecnico mi ha tolto tanto ma altrettanto mi ha dato e tu, senza dubbio, sei il regalo più grande che mi abbia fatto.

Grazie a Giulia, la mia costante, la compagna di una vita. Grazie perché "quando tutte le parole sai che non ti servon più" io so di poter contare su di te. Grazie per le coccole e le attenzioni, per le risate che solo con te sono così sincere. Il mio angelo custode sempre presente, la mia stella polare che mi guida brillando sempre, anche nelle peggiori tempeste. Sei il mio tutto.

Contents

Abstract **1**

1 Introduction **5**

1.1 Physical human robot interaction 7

1.2 Prior works 10

1.3 Thesis purpose 17

1.4 Contribution 18

1.5 Thesis structure 19

2 Admittance control: a geometrical interpretation **21**

2.1 Introduction 21

2.2 Admittance control: an overview 23

2.3 Admittance filter: a physical interpretation 29

3 Goal driven variable admittance control **33**

3.1 Introduction 33

3.2 Basic goal driven variable admittance control 35

3.3 Damping ellipsoid 40

3.4 Ellipsoid first principal axis direction 41

3.4.1 Minimum Curvature path 42

3.4.2 Minimum curvature path integration into the developed algorithm 47

3.5 Quadratic constraint optimization problem 49

4 Experimental results 53

4.1 Introduction 53

4.2 Experimental set-up 54

4.3 First test: objectives, set-up and outcomes 60

4.3.1 Outcomes 63

4.4 Unknown goal experiment: objectives, set-up and results 71

4.4.1 Outcomes 72

5 Conclusions 75

5.1 Future developments 77

Bibliography 82

List of Figures

1.1 Collaborative robot station 6

1.2 Example of physical interaction between a human operator and a robot 7

1.3 Example of manual guidance application 8

1.4 Quality inspection process using a collaborative robot physically interacting with the human operator 9

2.1 Admittance control and Impedance control input/outputs 22

2.2 Example of a body with mass M interacting with the environment 23

2.3 A representation of a one degree of freedom mass (M) - spring (k_1) - damper (k_2) system. 24

2.4 Admittance control scheme 26

2.5 Admittance control: schematised representation 27

2.6 Pictorial view of the space dependence of the admittance parameters in invariable admittance control 30

2.7 Representation of the geometrical interpretation of the mechanism of variation of the virtual parameters in a traditional variable admittance control fashion: the variation of the virtual parameters can be seen as an increasing/decreasing of the sphere radius . . . 31

3.1 Representation of the ellipsoid that defines the parameters space dependency. 35

3.2 High view - corresponding to a 2-dimensional analysis - schematised representation of the variation of the first principal axis of the ellipsoid, $\boldsymbol{v_1}$, when the relative position between $\boldsymbol{p_e}$ and $\boldsymbol{p_G}$ is changed . . . 39
3.3 Representation of the improved shape for the damping constituted by the union of two half-ellipsoids. . . . 40
3.4 Representation of the minimum curvature path and of the new ellipsoid first semi-axis direction. . . . 47
3.5 Representation of the operating space with some of the considered constraints, generating a forbidden area, represented in red. The end-effector of the manipulator must not enter into the red zones (both dashed and not) to not go into a failure state. . . . 50

4.1 IRB 140 manipulator equipped with a 6 axis Robotiq FT300 F/T sensor . . . 54
4.2 Workspace of ABB IRB-140 robot. . . . 55
4.3 Architecture of the industrial robot IRB 140. . . . 56
4.4 IRC 5 - Robot control unit . . . 57
4.5 Picture of the experimental set-up for the first set of experiments. 60
4.6 Statistics of the time needed to complete the path with the different control techniques. . . . 63
4.7 Statistics of the energy needed to complete the path with the different control techniques. . . . 64
4.8 Statistics of the positioning precision with the different control techniques. . . . 65
4.9 Statistics of the path length with the different control techniques. 66
4.10 Behaviour of the virtual damping in a normalised time scale for the IAF-L, IAF-M, IAF-H and VAF with its 75th and 25th percentile. 67

4.11 Zoom of the behaviour of the virtual damping in a normalised time scale for the IAF-L, IAF-M, IAF-H and VAF with its 75th and 25th percentile. 68
4.12 Questionnaire statistics of the effort perceived by the operators when using the invariant control techniques compared with the one perceived when using the variable strategy. The relative results are expressed in percentage. 69
4.13 Questionnaire statistics of the easy of approaching the goal position of the invariant control techniques with respect to the variable strategy. The relative results are expressed in percentage. 70
4.14 Statistics of the positioning precision in reaching the subsequent unknown random goal position. 72
4.15 Questionnaire statistics about the unknown goal approaching experience. 73

List of Tables

3.1 ABB IRB140 joints limits in minimum and maximum allowed displacements and in maximum velocities 49

4.1 D-H parameters for the robot. 56

Abstract

Nowadays, one of the most interesting and innovative topics in industrial robotics is represented by the collaborative interaction between human operators and robots. While in traditional robotics the manipulators are segregated into cages for safety reasons, in collaborative robotics human workers share the work station with robots, cooperating with them. In this way the high level of precision, speed and repeatability of the robots is combined with the flexibility and cognitive skills of human operators, speeding up the execution of the tasks, improving the quality of product, and decreasing the human effort.

In particular, a field where collaborative robotics finds application in is the so called *physical human-robot interaction* (***pHRI***).

Physical human-robot interaction has recently aroused growing interest among the scientific community: assistive technologies, collaborative industrial manipulators and rehabilitative robots are only few examples of this emerging technology.

The goal of the present work is to develop a variable admittance control for human-robot physical interaction in manual guidance applications. The task of the robot is to actively assist the human in moving an object from a starting load-position to a goal unload-position. In the proposed solution, the parameters of the admittance filter are changed not only as a function of the current state of motion (i.e. whether the human guiding the robot is accelerating or decelerating) but also with reference to a predefined goal position. The human is in fact gently guided towards the target along some curved paths, properly scaling the damping parameter to accommodate his/her motion. The developed algorithm also allows the human to reach goals that he/she cannot directly see because of, for example, the obstruction of his/her view caused by the bulky size of the transported object.

Eventually, the performance of the proposed controller are evaluated by means of point to point cooperative motions with multiple volunteers, exploiting an ABB IRB140 manipulator.

Sommario

Oggigiorno uno dei temi più interessanti e innovativi della robotica industriale è rappresentato dall'interazione collaborativa tra operatori umani e robot. A differenza di ciò che accade nella robotica tradizionale che prevede la separazione fisica tra l'operatore umano e il robot, il quale generalmente è confinato in una gabbia, nella robotica collaborativa l'operatore condivide lo spazio di lavoro con il robot, collaborando attivamente con quest'ultimo.

In questo modo l'elevata precisione, velocità, forza e ripetibilità che caratterizzano i movimenti dei robot si combinano con la flessibilità e le capacità cognitive proprie degli operatori umani. L'esecuzione dei vari compiti viene così resa più rapida ed efficiente, la qualità del prodotto viene migliorata e lo sforzo umano può essere notevolmente ridotto.

Una branca della robotica collaborativa prevede l'interazione fisica tra operatori umani e robot (**pHRI**). Quest'ultima ha recentemente suscitato un crescente interesse nella comunità scientifica: tecnologie assistive, manipolatori industriali collaborativi e riabilitativi sono solo alcuni esempi delle tecnologie emergenti.

In questa tesi si è sviluppato un controllo ad ammettenza a parametri variabili utilizzabile per applicazioni di guida manuale in cui il compito del robot è quello di assistere attivamente l'uomo nello spostamento di un oggetto da una posizione di carico iniziale a una posizione target di scarico. Nella soluzione proposta, i parametri del filtro d'ammettenza cambiano sia in funzione dello stato di movimento attuale dell'operatore umano che guida il robot (cioè se quest'ultimo sta accelerando o decelerando) sia con riferimento ad una posizione obiettivo predefinita. L'umano è infatti guidato dolcemente verso la meta seguendo alcuni percorsi curvi, grazie alla variazione dello smorzamento virtuale che viene opportunamente scalato al fine di favorire il movimento verso la posizione obiettivo prefissata. Inoltre l'algoritmo sviluppato consente all'operatore umano di raggiungere obiettivi che non sono visibili direttamente a causa, per esempio, dall'ingombro del carico trasportato che può causare l'ostruzione della visuale del lavoratore.

Infine, le prestazioni del controllore proposto sono state valutate da più volontari, mediante movimenti cooperativi, utilizzando un robot ABB IRB140.

Chapter 1

Introduction

One of the main objectives of the industry 4.0 is to increase the automation level of traditional industrial plants. A possible way to achieve this result consists in the introduction of *industrial robots* into the production chain. In particular, it is possible to distinguish between ***traditional robotics***, characterized by manipulators segregated into cages where humans were not allowed to enter for safety reasons unless all machines were stopped, and ***collaborative robotics***, in turn characterized by an active cooperation between human operators and robots. Indeed, even if robots were the core of many research activities and they found applications in industrial plants since many years, before the rise of the industry 4.0 they were mostly used to cyclically perform the same operations, generally requiring high speed and precision. However, in the last decade a growing interest in collaborative robots arose, so that it was possible to combine their capabilities with those of humans, obtaining the best from both of them [14].

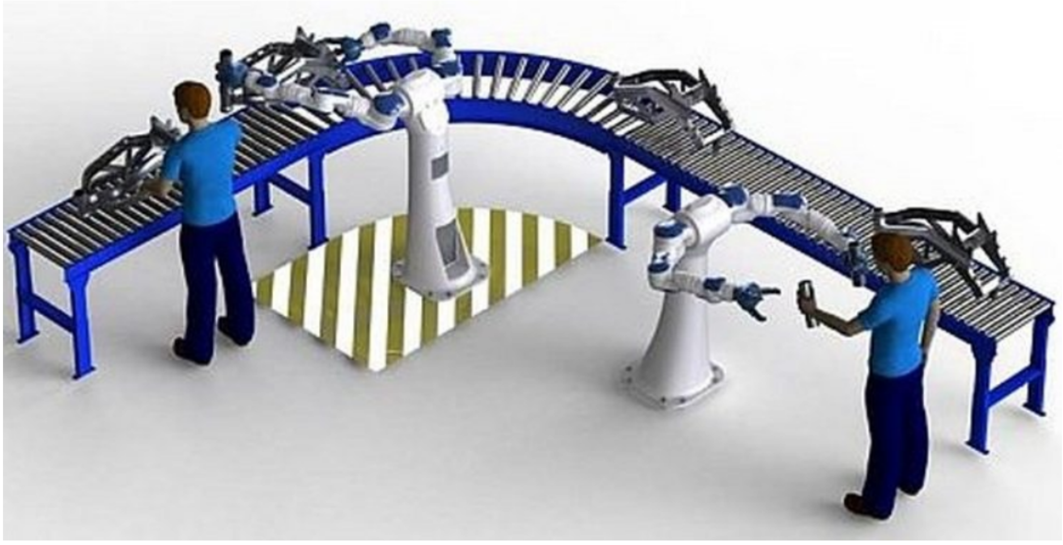

Figure 1.1: Collaborative robot station

Indeed, some of the actions which must be performed into a production line could be still too complex for a robot, while others could require a too high level of precision and repeatability, making them not suitable for humans. Within these application boundaries, collaborative robots can be seen, for all intents and purposes, as co-workers which help the human in the accomplishment of a wide variety of tasks, undertaking complementary actions [13]. Moreover, the application of collaborative robots, namely *cobots*, inside plants allows to save a lot of space since they don't have to be segregated. In addition, they are smaller, lighter, much more flexible and easily reconfigurable with respect to the traditional, expensive, huge and specialized ones. For these reasons, *cobots* are more attractive than traditional robots.

In order to allow the introduction of manipulators into plants populated by humans, they must be designed with sensors and intrinsic safety features, such as force feedback and collision detection, so that operators can work safely alongside them [4]. Despite bringing new challenges and safety issues since, as previously mentioned, humans and robots are no longer separated by a physical barrier, collaborative robots provide the production lines with huge benefits: mixing robots force, speed and accuracy with human intelligence and manual skills improves not only the industrial processes, but also the health of the worker, whose fatigue and alienation associated with the execution of repetitive tasks are thus reduced.

1.1 Physical human robot interaction

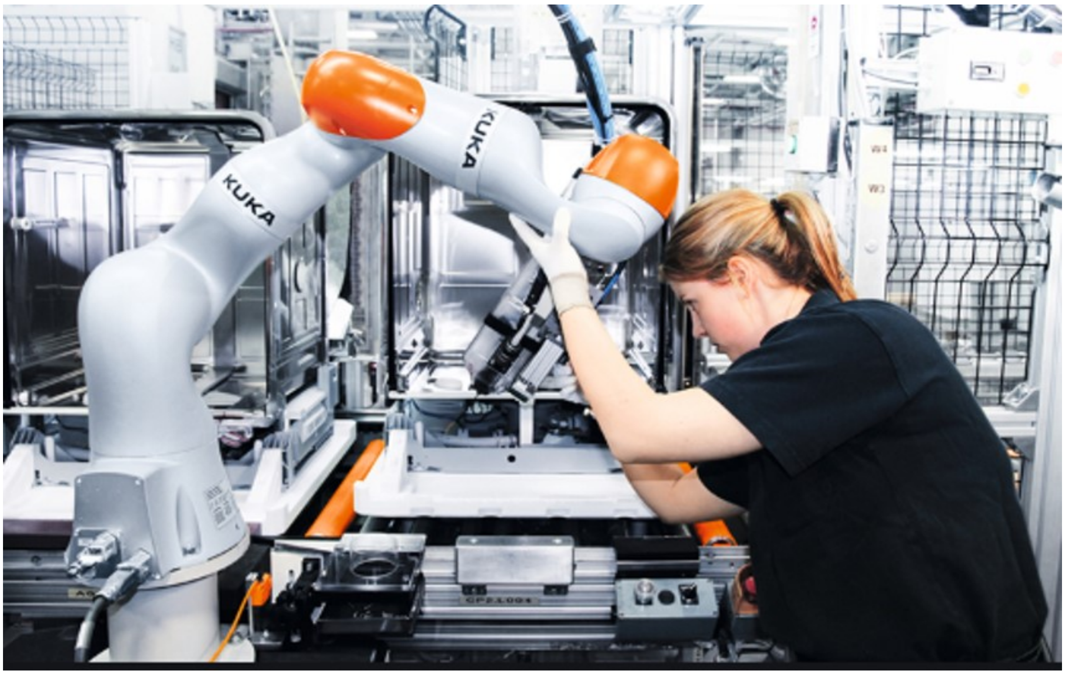

Figure 1.2: Example of physical interaction between a human operator and a robot

Although the boom in the use of collaborative robots can be placed in 2017, and therefore it is a relatively recent phenomenon [2], nowadays they dominate the robot market and by 2021, the number of units in the world is expected to grow to about 2.5 billion. In particular, all the applications involving the physical contact between the human operator and the manipulator represent a highly important sub-field of collaborative robotics. Indeed, as previously mentioned, the introduction of *cobots* in plants brings a significant increase to both the automation level and efficiency of industrial production lines.

In order to better understand the fundamental role of this technology, some tasks involving the physical interaction between robots and human operators will be mentioned in the following, even if a complete classification (also involving non-industrial applications) is practically unfeasible due to the large variety of cases that may occur.

Pick and place together with ***packaging and pelleting*** are activities in which a piece is first loaded and then placed in a different location. These kind of tedious, highly repetitive and alienating operations, if performed by a human operator, can often lead to mistakes and also be the cause of possible stress and injuries due to the weight and the dimension of the object being transported.

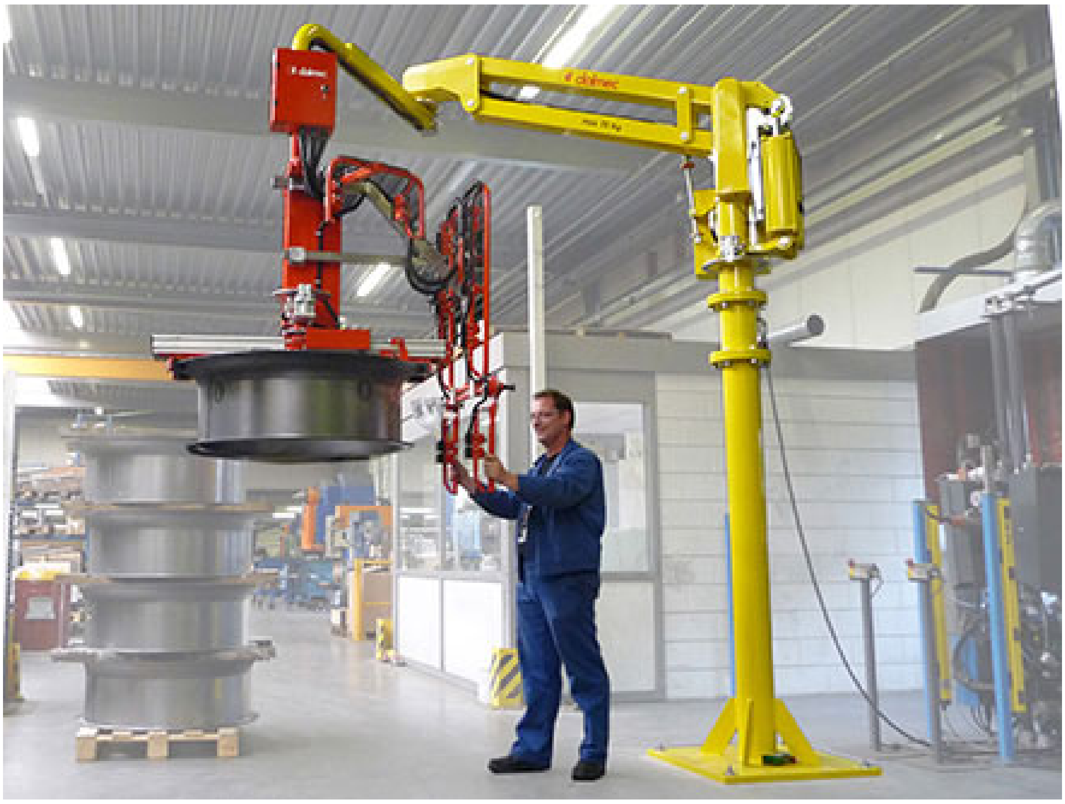

Figure 1.3: Example of manual guidance application

In this context, the role played by **hand-guidance** (see Fig. 1.3), namely a collaborative operation allowed by safety standards, is central. Its typical application is the handling of large and heavy loads that humans are not capable of lifting up standing alone: on the one hand, a robot compensates for the gravitational load of the transported object, on the other hand the operator simply guides the robot end-effector to the right place, overcoming the non-negligible inertia load.

A further possible scenario of collaborative robotics application is constituted by ***quality inspection*** of parts, depicted in Fig. 1.4.

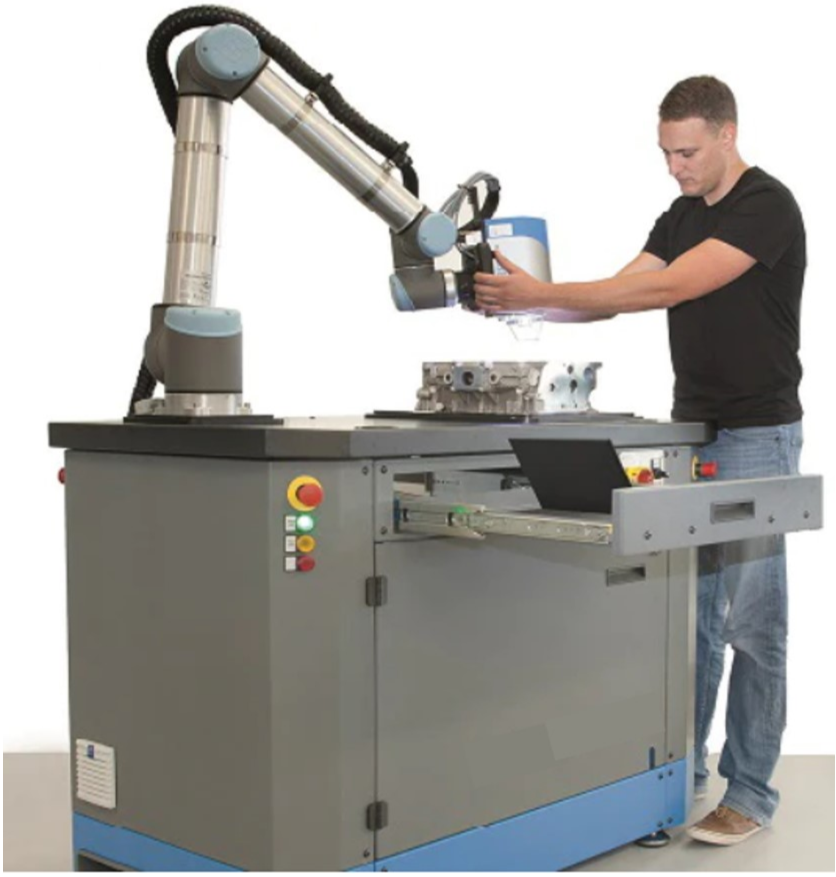

Figure 1.4: Quality inspection process using a collaborative robot physically interacting with the human operator

This process usually involves the full analysis of finished parts, the production of high resolution images for precision machined pieces and their verification against CAD models. Using cobots for inspection can bring to a higher-quality production batches.

Despite being the most noticeable and well known context, the industrial framework is not the only one collaborative robotics can be applied to. Physiotherapy and rehabilitative purposes are just two examples of how wide its sphere of interest is.

Among the benefits brought by the use of *cobots*, there is the improvement of the ergonomics of workstations which consequently increases industries productivity and allows for the relief of the ***human fatigue*** in terms of workload, one of the main scope of *pHRI*. To better understand how much human fatigue affects productivity in a plant, the following example could be valuable: suppose that a human operator has to move a heavy piece from a loading point to an unloading station, a typical illustration of a **pick and place** task. This kind of operation can be *tough* for the worker from a physical point of view, since bio-mechanical stresses, possibly causing injuries in the long run, are produced. Clearly these adverse working conditions, caused by the high level of fatigue gathered by the operators, are a disadvantage for the ergonomics of the workstation, which is representative of the strength of the whole company production line. Therefore, the use of articulated systems, *i.e.* manipulators, compensating for the objects weight and consequently relieving the human fatigue turns out to be essential.

1.2 Prior works

Over the last 40 years, the impact of robots on human life has significantly increased: advances in mechatronics and robotics have enabled the development of many machines capable of supporting human beings in an increasing number of activities. The capabilities of robotics have moved from simple operations to more advanced and difficult tasks, leading to significant improvements in many different fields. Nowadays, many efforts are focused on handling tasks involving the dynamic interaction between the robot and the external environment, as they would open up new and fascinating perspectives.

The dynamic coupling between the manipulator and the environment generates reaction forces that must be managed correctly in order to avoid undesirable effects. Pure position control fails in such context, since the contact forces lead to deviations from the desired trajectory the control system tries to compensate for. As a result, an accumulation of such forces occurs, until the robot hardware or the manipulated object breaks down. For these reasons, the interaction between the robot and the environment cannot be managed with traditional control techniques imposing a desired trajectory, but a peculiar interaction control has to be adopted.

Hogan [15] gave a contribution of historical importance in addressing the problem of controlling a manipulator in applications where it physically interacts with the environment. He proposed a method based on the dynamic coupling between robot and environment, known as **impedance control**. It is focused on controlling the dynamic relationship between the robot end-effector position and the interaction force exchanged with the environment, which is represented by the human arm in the present work.

An impedance control algorithm can be implemented in two different ways, depending on its application. It is possible to distinguish between the so-called "**impedance control**", which takes a displacement as input and gives a force as output, and the "**admittance control**", whose input and output are a force and a displacement respectively [18]. To properly work, both these control methods require the knowledge of the interaction force exchanged with the environment. Such force can either be measured by means of a force/torque sensor mounted on the robot end-effector or it can be estimated through different model-based or data-driven approaches.

In manual guidance applications, in order to make the robot compliant with the force applied by the human, an admittance control is typically implemented on the machine. This technique, as previously stated, simply converts the human force into a reference speed and position for the robot end-effector, which are then managed by the low level position and velocity axis control of the robot. The aforementioned conversion is realized by the so called **admittance filter**, thanks to which the end-effector of the manipulator behaves as a **mass-spring-damper** system when interacting with the environment. In particular, the mass corresponds to the one perceived by the operator when moving the end-effector of the manipulator, the damping represents the amount of resistance that the operator will perceive while moving the end-effector, and the stiffness term provides an attractive/repulsive contribution. In human-guidance applications, the stiffness term is usually not needed since a desired equilibrium position is not set: hence, only the mass and damping parameters are of interest.

Considering a one-dimensional admittance filter without the elastic term, the reference trajectory followed by the end-effector can be described as a desired position $x_d(t)$ and as a desired velocity $\dot{x}_d(t)$, expressed in the *Laplace domain* as follows:

$$\dot{x}_d(s) = \frac{1}{(ms + d)} f_H(s) \tag{1.1}$$

$$x_d(s) = \frac{1}{s(ms + d)} f_H(s) \tag{1.2}$$

where $x_d(s)$, $\dot{x_d}(s)$ are referred to the Laplace transform of the desired position and velocity of the end-effector respectively, $f_H(s)$ is the Laplace transform of the human force, s is the Laplace variable and finally m and d represents the **virtual mass** and **damping** respectively, which correspond to the mass and damping perceived by the human operator when interacting with the manipulator end-effector.

Linear, fixed-gain admittance filters, however, entail a trade-off in the achievable performance: according to the related studies available in literature, [19], [17], [9], the use of small virtual parameters leads to fast motions with low precision and low human-effort, while large virtual parameters guarantee precise motion but slow movements and high level of human fatigue.

Obviously, it is desirable that the control law exhibits the appropriate behavior depending on the working situation. For this reason, several researchers implemented different algorithms under the name of **variable impedance/admittance control**, trying to estimate the will of human motion and changing the virtual parameters accordingly. The underlying idea can be summarized as follows:

- During the **acceleration** phase, since the reduction of any resistance to the motion is advisable, the values of both the mass and the damping parameters are decreased;

- In case of **cruise speed**, a decrease of the damping parameter is advisable since it has a predominant role with respect to the the mass. Indeed, the higher the velocity, the bigger the resistive effect of the damping.

- During the **deceleration** phase, a reduction of the virtual mass and an increase of the virtual damping is advisable. Indeed, doing so, the braking phase is facilitated since the inertia counteracting the braking motion is reduced while the damping, which helps it while stabilising the system, is increased.

Generally, variable impedance/admittance control performs better than the constant parameters ones: it preserves the characteristic accuracy of the high parameters admittance filters and, at the same time, it guarantees fast movements with a lower level of human fatigue, proper of the low parameter ones.

As previously mentioned, one of the reasons related to the use of a variable impedance/admittance control is to accommodate the human movement during physical interaction with robots, in order to improve his/her feeling while performing a specific task (*e.g.* transportation of heavy loads), paving the way to different methods of tackling the problem.

In [12], a variable impedance control is adopted to manage the robot during the physical interaction with the human operator. The impedance parameters were adapted online, during the interaction, according to the human behavior, which was inferred by measuring the end-effector velocities. The best results in terms of stability and performance are obtained in case of a variable damping and of a constant virtual mass set to its minimum value, compatibly with the stability requirements.

Ikeura et al. [16] in turn presented a very simple variable admittance control, consisting of two different invariable admittance controls, one for low velocity and the other one for medium and high speed.

In [17], the researchers pointed out that in order to make robots human-friendly it was important to design the controller considering also the human arm characteristics. The most appropriate way for describing its dynamic behavior is represented by a mechanical impedance (*i.e.* stiffness, viscosity and inertia). The human arm is modelled as a pure damper and the model parameters are fitted by means of a recursive least square procedure. The estimated relation is then used as an admittance control for the robot.

In [22], the operation is divided into four subsequent phases, each of which is defined by a passivity index measuring the energy transfer occurring between the operator and the robot during the cooperation work. In case of a positive index exceeding a given threshold, the worker gives energy to the robot. Moreover, each phase is associated with a specific set of virtual parameters, whose assigned values correspond to either the minimum, the nominal or the maximum.

In [23], the attention is drawn to low velocity situations, simply approximating the human impedance by means of a spring. Furthermore, the stiffness of the human arm is estimated online, while the damping of the robot for slow motion is proportional to the stiffness itself.

Duchaine et al. [8] proposed a law that varies the damping proportionally to the derivative of the force applied by the human, projecting it along the speed of the end-effector. A sudden increase in force magnitude along the direction of the velocity could be interpreted as a human intention to accelerate, therefore the damping coefficient should be reduced. On the contrary, a sudden decrease in force magnitude along the direction of the velocity could be interpreted as an intention of the human to decelerate, stop the movement or reverse the direction of motion, making both a high damping coefficient and a reduction of the virtual inertia desirable. Such observations were included into the conventional impedance control low, applying a weighting factor to the force derivative.

In [3], the damping is varied with the end-effector velocity in a inversely proportional fashion.

In [19], a variable admittance control, whose parameters are changed according to the inferred human intentions, is presented. The human will to accelerate or decelerate is first estimated by comparing the acceleration and speed signs, the damping parameter is then varied proportionally to the acceleration module and the mass parameter is changed in order to keep the bandwidth of the admittance filter constant, making the interaction more intuitive from the operator point of view.

The topic of variable admittance control has been also faced by some more recent works, exploiting machine learning techniques [6], [5]. The objective is to find the best set of parameters for a specific person in order to suitably adapt to him/her during a task along a predefined linear path.

In [20], a multi-layer feed-forward neural network, establishing the damping value in response to both a certain end-effector velocity and a human force, is presented. Further investigations have been conducted to select the best set of virtual parameters able to avoid the rise of oscillations at the end-effector.

According to [19], [17], [9], the human perception is mainly influenced by the damping parameter, while in [24] it is shown that, for a given damping, the desired virtual mass is of crucial importance for stability reasons: to avoid instabilities, the minimum achievable virtual mass has to be set approximately $6 \div 10$ times lower than the actual mass, while no maximum value is defined.

Additionally, according to [19], if the virtual mass is kept constant, as in [17], [16], [23], [8], [22], some undesirable effects occur. On the one hand, when an acceleration is desired, the gain obtained by decreasing the virtual damping will be partially cancelled, since the virtual mass to virtual damping ratio will increase significantly, slowing the response down. On the other hand, in case of a deceleration, the virtual mass to virtual damping ratio will decrease due to high damping. Therefore, depending on the current damping value, a stability zone is experimentally identified, so that the operator can be led to work in vibrations-free conditions.

Another possible cause of instability during the *pHRI* is investigated in [21] and it is found to be due to the coupling between the robot and the human operator. If he/she stiffens too much his/her arm, deviations from the nominal behavior could arise, producing highly amplified oscillations which can render the interaction unsafe for the user.

In [7], a frequency domain analysis is adopted to distinguish the unstable motion due to unwanted oscillations from the voluntary one. This was possible since the bandwidth of the human arm during voluntary motions is below 2Hz, while the frequencies of the robot oscillations are higher and easily recognizable. An online recursive instability index was built in order to quickly detect the amplification of oscillations before becoming noticeable by the operator. Successively, the admittance parameters were tuned, changing them proportionally to the instability index, until the oscillations completely disappeared. This study also focuses on the high increase of the fatigue perceived by the operator if oscillations are dissipated by increasing the virtual damping parameter (traditional method). Indeed, if the operator interacts with the robot at a relatively steady velocity, a further increase of the virtual damping, representative of the dominant perceived forces, will affect the operator's effort during the entire motion. On the contrary, only in case of acceleration and deceleration, an augmentation of the inertia should be preferred since it is perceived by the operator as a higher reaction force, facilitating a low-effort cooperation.

The variation of the virtual parameters according to the spatial direction of the applied force is still an unexplored field, but could be very useful in applications where the goal position is known, which is the case of the present work.

1.3 Thesis purpose

The main purpose of the current work is the development of a variable admittance control for human-robot physical interaction in manual guidance applications, where the admittance parameters are varied according to the direction of the applied human force and of the goal end-effector position with respect to the actual one.

This latter dependency could be obviously very functional in case the human will is to reach a precisely known goal position. As a matter of fact, with the existing solutions the problem of directing towards a specific goal has always been in charge of the human. This can be a challenging task if the transported object has a big inertia and/or a big size that prevents the human from viewing the target position.

Therefore, in this work, a variable admittance control that gently helps the human operator in directing towards the predefined goal position, also along a possibly curved path, is developed. This new additional function has also the classical objectives of reducing both human effort and task execution time while maximizing the accuracy in positioning the end-effector in proximity of the target.

1.4 Contribution

A new physical interpretation of the admittance filter is presented, extending the classical one. This allows to implement variable admittance filters able to overcome the classical trade-off described in literature, ensuring at the same time an active assistance to the human beings in directing towards a specific goal position, also following non linear paths (up to now, the majority of the existing algorithms only refer to linear paths). Indeed, in the developed algorithm, the admittance filter parameters have been changed taking into account the current state of motion of the human operator with reference to a predefined goal position. In this way, the human is guided towards the target, following a curved path, thanks to a convenient variation of the damping virtual parameter. The implemented algorithm also finds application in the case in which the worker must load, transport and finally unload a bulky object in a prescribed position. In this context, the operator's view can be obstructed by the surface of the transported load. For this reason, the worker could experience several issues in choosing the right direction of motion to reach the target position. Such difficulties can be overcome endowing the manipulators with an algorithm, as the one developed in this thesis, that makes the worker perceive different sensations depending on the direction of the force applied by them. In particular, the damping parameters have been increased when the human direction of motion results to be different from the suggested one. At the same time, the damping parameter will be also increased if, once the goal position is reached, the operator deviates from it. By doing so, the human worker will maintain his/her autonomy in choosing the direction of motion, being however gently guided to the target position. Thanks to the implementation of this innovative technique, not only the operator will be assisted in the task execution but also his/her fatigue will be mitigated.

1.5 Thesis structure

In this section, the description of the thesis structure is provided.

- **Chapter 2**: a review of the classical admittance control together with the explanation of its physical meaning is provided. The concept of variable admittance control is then introduced, highlighting the reasons why it is of crucial importance when dealing with physical human-robot interaction. Eventually, a first insight into the innovative interpretation of the admittance control technique, which is the basis for the current project, is given.

- **Chapter 3**: all the preliminary steps needed to structure the proposed algorithm are presented. Then, the various parts composing such algorithm are faced one after the other. The idea and the procedure at its basis are summarized: in a first instance, the most basic case of application is explained, further discussing its improvements into details. Hereafter, the concept of the minimum curvature path and its usefulness for the developed algorithm are presented. The chapter ends with the explanation of the reason why a quadratic constrained optimization problem has to be faced.

- **Chapter 4**: the effectiveness of the developed algorithm is shown through the analysis of the experimental results. Firstly, the experimental set-up is discussed. Secondly, two different experimental tests are described: on the one hand, the algorithm is applied to a real manual guidance case with a known goal position and its performance, in terms of completion time, positioning precision, path length and required human energy, are compared with traditional techniques. On the other hand, the tester is asked to move the end-effector so as to reach, as precisely as possible, an unknown goal which cannot be seen, only relying on the directional feedback returned by the proposed algorithm. Finally, the results of these two experiments are shown and analysed.

- **Chapter 5**: final remarks and hints about possible future developments and improvements to the implemented algorithm are discussed.

Chapter 2

Admittance control: a geometrical interpretation

2.1 Introduction

As pointed out in Chapter 1, since an increasing number of activities require the support of robots, control strategies allowing a stable interaction between manipulators and the surrounding environments have long been investigated. Indeed, in such context, pure *position control* fails because of the existence of the dynamic couplings between the manipulator and the environment which generates reaction forces that, if not managed correctly, can bring unwanted effects. This happens since the contact forces lead to deviations from the desired trajectory that the control system tries to compensate for, bringing, as a result, an accumulation of such forces until the robot hardware or the manipulated object breaks down. For these reasons, since the interaction of the robot with the environment cannot be managed using traditional control techniques, which impose a desired trajectory, a peculiar interaction control has to be adopted.

The *compliance control* refers to a family of control strategies using the force feedback to define a target dynamic behaviour of the controlled robot instead of exploiting it to directly calculate the control action, as it occurs with *force* and *hybrid* control strategies. Indeed, when the manipulator is interacting with an unknown environment, represented by the human operator in the case of interest, it could be not trivial to set a reference force to achieve a target interaction. For this reason, in such applications an evolution of the previously mentioned control strategies, represented by the so called *impedance control*, is taken into account [15].

In particular, two main control strategies can be defined:

- Impedance control
- Admittance control

These two control strategies differ for the causalities of their controller, as shown in Fig. 2.1.

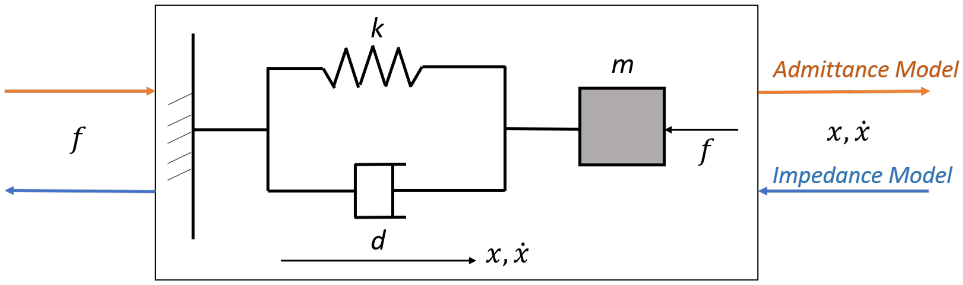

Figure 2.1: Admittance control and Impedance control input/outputs

Indeed, considering the impedance control, the controller is represented by an impedance (*i.e.* a physical system accepting a motion as input and giving a force as output) and the manipulator is an admittance (*i.e.* a system accepting a force as input and yielding a motion as output). So, basically, the use of an impedance control implies the exploitation of positions, speeds and accelerations to control the drives by means of torques and forces. On the contrary, in the admittance control the controller is an admittance and the manipulator an impedance.

Moreover, it is known from literature that the impedance control is characterised

by a stable dynamic interaction with stiff environments and poor accuracy in free space due to unmodeled dynamics. In contrast, admittance control provides high level of accuracy in non-contact task but its use brings to instabilities when dynamic interaction with stiff environment occurs.
Since in this work a manual guidance task, *i.e.* a free motion application, is considered, this chapter will focus on the description and analysis of the **admittance control**, which represents the adopted control technique.
Hereafter, an innovative interpretation of such control strategy, constituting the core of the present research, is provided.

2.2 Admittance control: an overview

In order to understand how an admittance controller operates, it is worth to analyse the system depicted in Fig. 2.2: it consists of a single degree of freedom system, composed by a mass M interacting with the external environment, exerting a force f_{ext} on the mass itself [10].

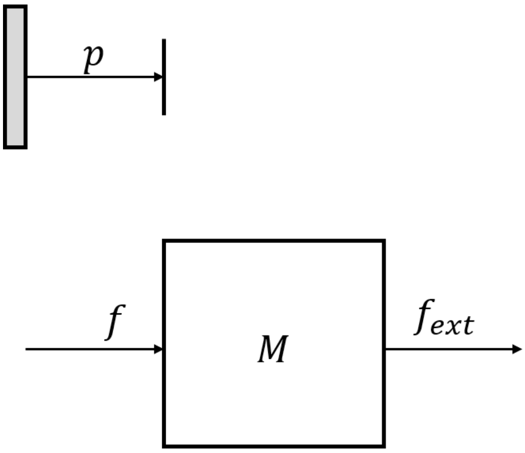

Figure 2.2: Example of a body with mass M interacting with the environment

The system is described by the following equation:

$$Ma = f + f_{ext} \tag{2.1}$$

where M and a are the generalized inertia and acceleration of the mass respectively, f corresponds to the control action and f_{ext} is the external force exerted by the mechanical environment on the mass.

If a control proportional to velocity k_1 and position k_2 is applied, the following control action is obtained:

$$f = -(k_1 v + k_2 p) \tag{2.2}$$

where v is the velocity and p the position of M.

Substituting Eq. 2.2 into Eq. 2.1, it results:

$$Ma + k_1 v + k_2 p = f_{ext} \tag{2.3}$$

From equation 2.3, it is clear that the controlled system reacts to the external force like a **mass-spring-damper system** (Fig. 2.3).

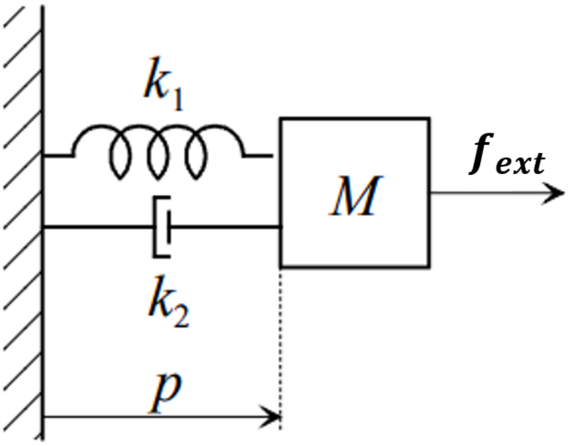

Figure 2.3: A representation of a one degree of freedom mass (M) - spring (k_1) - damper (k_2) system.

k_1 and k_2, namely the damping and stiffness coefficients, are tunable while M, *i.e.* the physical mass of the system, in this case cannot be changed.

In order to make also the value associated to the physical mass of the system tunable, it is necessary to measure the external force acting on the system itself, so that the following control action is obtained:

$$f = \frac{M}{M_d}(-k_1 p - k_2 v + f_{ext}) - f_{ext} \tag{2.4}$$

Substituting Eq. 2.4 into Eq. 2.1, it results:

$$M_d a + k_1 v + k_2 p = f_{ext} \tag{2.5}$$

Hence, the mass-spring-damper system parameters are now all tunable.

Implementing an impedance or an admittance control, the end-effector of the manipulator interacting with the environment, that in the case of interest is represented by a human hand applying the external force f_{ext} at the interface, behaves like a mass-spring-damper system and both controllers should provide an action force satisfying Eq. 2.5, which relates the external force with system dynamic quantities.

When dealing with impedance/admittance control, k_1 and k_2 correspond to the so called *virtual damping* (D_d) and *stiffness* (K_d) parameters, respectively. Furthermore, the *virtual mass* M_d represents the mass perceived by the operator when moving the end-effector of the manipulator, the virtual damping represents the amount of resistance that the operator will perceive while moving the end-effector of the manipulator and the virtual stiffness provides an attractive/repulsive contribution.

Substituting a, p and v with the corresponding errors computed with respect to a steady state equilibrium position of the system, the following relation is obtained:

$$M_d \ddot{e} + D_d \dot{e} + K_d e = f_H \tag{2.6}$$

where, as previously mentioned, M_d, D_d and K_d are positive constants representative of the desired inertia, damping and stiffness of the system, f_H is the external force applied by the human, $\ddot{e}$, $\dot{e}$ and e are the acceleration, velocity and position errors respectively.

Moreover, the position error is defined as:

$$e = x - x_0 \tag{2.7}$$

where x_0 represents the nominal equilibrium position at steady state.
Eq. 2.6 defines a mechanical impedance relation between the forces/moments and the position/orientation errors in the operational space, allowing to define the system dynamic behaviour along each direction of the work space.
A deeper explanation of the admittance control technique, which is the control strategy adopted in this work, is hereafter presented.
According to Eq. 2.1, the aim of the admittance control is to design a control force f capable of establishing a relationship between the external force f_{ext} applied by the environment, *i.e.* the human operator, and the deviation from a desired equilibrium position, x_0. Therefore, the admittance control converts an external force into a desired displacement, as observable from Fig.2.4.

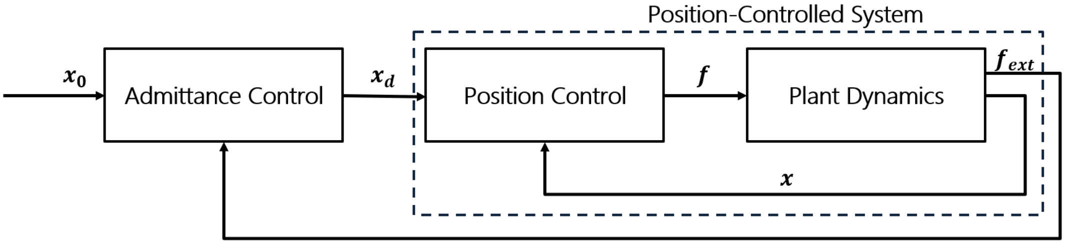

Figure 2.4: Admittance control scheme

Moreover, as shown in Fig.2.4, since when dealing with industrial manipulators a direct access to the joint torque commands is not available, it is possible to modify the reference position relying on a stiff position control exploiting an implicit control scheme, as the one depicted.
Since a manual guidance task (*i.e* a free motion application) is considered in this framework, the virtual stiffness parameter K_d, whose function is to attract the end-effector of the manipulator towards a desired pose, together with the starting position x_0, velocity $\dot{x_0}$ and acceleration $\ddot{x_0}$, are set equal to zero.

Hence, Eq. 2.6 becomes:

$$M_d \ddot{x}_d + D_d \dot{x}_d = f_H \tag{2.8}$$

Moreover, the reference trajectory followed by the end-effector can be described either with a desired position x_d or a desired velocity $\dot{x}_d$.

Defining Eq. (2.8) in the *Laplace domain*, the desired velocity can be written as:

$$\dot{x}_d(s) = \frac{f_H(s)}{M_d s + D_d} = \frac{1/D_d}{\frac{M_d}{D_d} s + 1} f_H(s) = H(s) f_H(s) \tag{2.9}$$

Hence, the desired position results in:

$$x_d(s) = \frac{f_H(s)}{s(M_d s + D_d)} \tag{2.10}$$

where $x_d(s)$ and $\dot{x}_d(s)$ are the Laplace transforms of $x_d(t)$ and $\dot{x}_d(t)$, while $f_H(s)$ is the Laplace transform of $f_h(t)$.

Analyzing $H(s)$, it is observable that the virtual damping affects the steady-state value of the response while the virtual mass to virtual damping ratio affects the dynamics, as it changes the pole of the first order system.

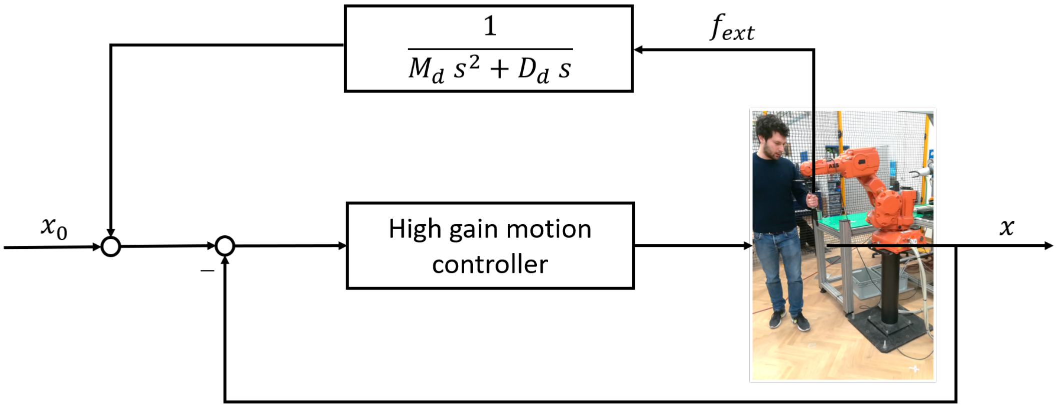

Figure 2.5: Admittance control: schematised representation

Moreover, as previously explained, if during the interaction an admittance control is applied, the human operator perceives to move a mass M_d with a damping D_d and the variation of their assigned values will also influence the operator's feeling. For this reason, the *virtual mass* and *virtual damping* parameters are associated with high values when the operator wants to perform fine and precise movements, making the robot less reactive and the interaction smoother. On the contrary, when they are set to low values, it is easy for the human operator to move the robot at high velocity and with high acceleration, but precise movements are quite difficult to be performed. As a consequence, the use of linear, fixed-gain admittance filters entails a trade-off in the achievable performance which represents the main **drawback** of a ***fixed*** **admittance control**. Indeed, it is desirable that the implemented control law exhibits the appropriate behavior depending on the working condition. For this reason, since the early '90s, several researchers have proposed different algorithms under the name of ***variable*** **impedance/admittance control**, trying to estimate the human will of motion and to change the virtual parameters accordingly. Basically, three different phases can be distinguished in the human operator motion: the acceleration, the cruise speed and the deceleration. During the first one, both the mass and the damping are reduced since they represent a resistance to the motion. In case of cruise speed, instead, a reduction of the damping parameter is advisable, since it has a predominant role with respect to the mass. Doing so, in both phases, the operator could move the end-effector of the manipulator with low efforts. Moreover, in order to facilitate the braking phase, a reduction of the virtual mass, which counteracts the braking motion, and an increase of the virtual damping, which helps the braking action, is advisable. During the deceleration phase, the operator will be still subjected to a lower level of fatigue with respect to the case where high fixed virtual parameters are used, and, at the same time, a good level of positioning accuracy will be guaranteed.

It is possible to conclude that the variable impedance/admittance control performs better than the constant parameters ones. Indeed, it combines the accuracy proper of high parameters admittance filters with the lower level of human fatigue and faster movements guaranteed by low parameter ones.

2.3 Admittance filter: a physical interpretation

This section introduces the concepts at the basis of the proposed extended physical interpretation of the admittance filter.

To do so, a one-dimensional admittance filter without the elastic term, for the reasons explained in Sec. 2.2, can be taken into account:

$$v = \frac{1}{Ms + D} f \tag{2.11}$$

where M and D are the virtual mass and damping respectively perceived by the human when a force f is applied in correspondence of the end-effector and v is the reference speed for the robot tool frame.

The relation expressed with Eq. 2.11 can be extended to the 3-dimensional case, adopting an admittance filter for each force component in a decoupled fashion:

$$v_x = \frac{1}{M_x s + D_x} f_x \tag{2.12}$$

$$v_y = \frac{1}{M_y s + D_y} f_y \tag{2.13}$$

$$v_z = \frac{1}{M_z s + D_z} f_z \tag{2.14}$$

where v_x, v_y and v_z are the Cartesian components of the speed vector $\boldsymbol{v}$ and f_x, f_y and f_z are the ones of the applied force $\boldsymbol{f}$.

As reported in literature, the parameters of the three filters must be set equal the one to the other, so to preserve a natural interaction between humans and robots. Therefore, the relationship between force and speed in a 3-dimensional space can be re-written as follows:

$$\boldsymbol{v} = \frac{1}{ms + d} \boldsymbol{f} \tag{2.15}$$

From this equation it is possible to understand that the velocity vector will have the same direction of the force with filtered amplitude, meaning that, if the force $\boldsymbol{f}$ applied by the human had a constant direction (or slowly varying with time), the filter in Eq. 2.15 would not change it.

The idea is hence to associate each parameter characterizing the admittance filter to the spatial direction of the human force.

The value of every aforementioned parameter can be represented by the radius of a sphere, centred in the origin of a reference system defined at the end-effector of the manipulator and whose axes are set parallel to those of the global reference system (Fig. 2.6).

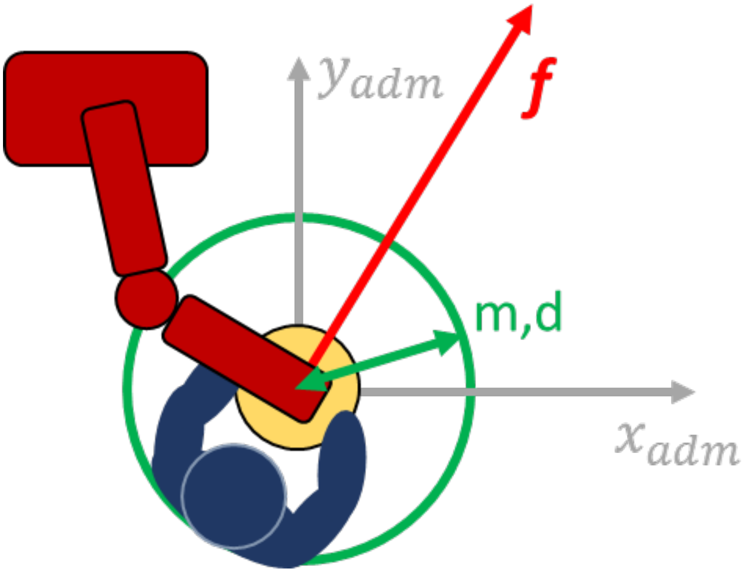

Figure 2.6: Pictorial view of the space dependence of the admittance parameters in invariable admittance control

In all the variable control techniques developed over the years, the virtual parameters have always been changed according to scalar functions, depending either on the intensity of the applied force, acceleration and/or speed or on the estimation of the stiffness and damping parameters related to the human arm.

Making a parallelism with the graphical interpretation explained above, these methods of variation of the admittance filter virtual parameters are equivalent to the modulation of the radius of the sphere, without providing any directional information (Fig. 2.7). Thus, a change in the sphere radius allows to vary the parameters characterizing the admittance filter.

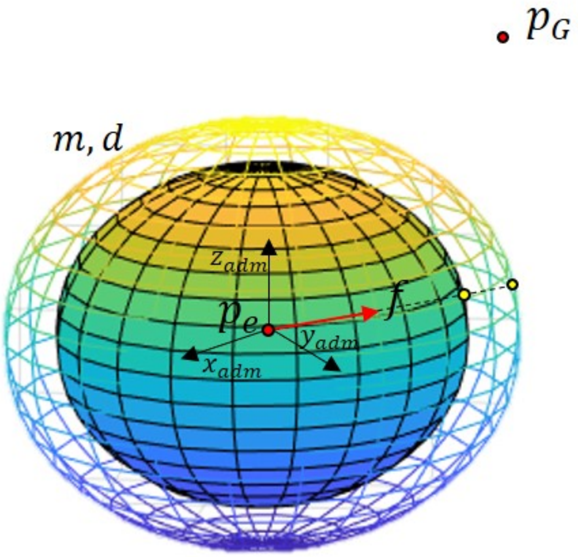

Figure 2.7: Representation of the geometrical interpretation of the mechanism of variation of the virtual parameters in a traditional variable admittance control fashion: the variation of the virtual parameters can be seen as an increasing/decreasing of the sphere radius

The aim of Fig. 2.7 is to underline the mechanism of variation of the virtual parameters when a traditional admittance control technique is implemented.
p_e represents the actual position of the end-effector of the manipulator while p_G corresponds to a target position. Mixing the provided geometrical interpretation with the variable admittance control techniques developed up to now, when the admittance parameters are changed (for example in accordance to a velocity variation) the values associated to the virtual damping and inertia could be computed as the intersection between the direction of the applied force and the sphere surface, which corresponds to the length of the sphere radius.
The variation of virtual parameters, *i.e.* of the radius, results in two concentric spheres: the yellow points marked on their surface are representative of the in-

tersection points of the spheres with the direction of the human force. The value of the parameters is then equal to the distance between the corresponding yellow points and the origin of the sphere. Since the radius of a sphere is constant in any direction, the corresponding virtual parameters are changed independently from the direction of application of the human force, *i.e.* whether or not he/she is moving towards the target position.

Now, considering a manual guidance application and supposing that the target position is known, the main idea is to modulate the gains of the admittance filter in Eq. 2.15 in such a way that the human feels more comfortable when moving towards p_G, without however constraining the motion to an assigned path.

Consistently with the current geometrical interpretation, a 3-dimensional shape has to be introduced, which depends on the relative orientation between the applied force and the direction towards the goal position. The parameters of such 3-dimensional volume will be used to suitably modulate the gains of the admittance filter, as it will be explained in the next chapter.

Chapter 3

Goal driven variable admittance control

3.1 Introduction

In Chapter 2, the explanation of the theoretical concepts at the basis of the developed algorithm along with an innovative interpretation of the *invariant admittance control* have been provided. The values of its virtual parameters could be associated to the radius of a sphere (see Fig. 2.6) centred in the origin of the local frame of reference (defined in correspondence of the robot end-effector), whose axes have the same orientation of the ones belonging to the global frame (defined in correspondence of the robot base).

Moreover, it has been highlighted how, in previous works, the virtual parameters of the admittance filters have been just varied according either to the inferred operator's intentions to accelerate/decelerate or to the intensity of the force applied by the operator himself/herself to the end-effector, without considering neither the direction of such force nor the goal position.

The need to account for these parameters becomes particularly evident whenever a human worker carries a bulky object: its huge dimension could prevent the operator from having a clear view of the operating space, making the positioning task quite challenging and hard to be performed. This is the context where the presented interpretation of the variable admittance control technique finds application in. Indeed, supposing that the goal position is known, the main idea is to modulate the gains of the admittance filter accordingly. In this way, thanks to the developed algorithm, the human will be more comfortable when moving towards the goal, without however being deprived of his/her autonomy in choosing the path to be followed to get to the target position.

In order to reach this purpose, the sphere, previously introduced in Sec. 2.3 as the geometrical shape apt to describe the invariant admittance control technique, is then deformed in an **ellipsoid**.

While the sphere is characterized by three axes with the same lengths, making it a suitable 3-dimensional shape for the representation of the invariant admittance control technique, the ellipsoid, a particular type of quadratic corresponding to the 3-dimensional analogue of the ellipse, is a closed second order surface with three axes of symmetry of independent length.

The ellipsoid will be centered in the local frame of reference, as the sphere was, but its axes will have a specific direction in the 3-dimensional space. The selection of the axes directions and lengths will allow the human operator to perceive different efforts, depending on the direction of the applied force with respect to the goal position. This will provide the operator with a sort of natural feedback, allowing him/her to reach the goal even in case of obstructed view.

Adopting the described approach, the operator will thus be assisted during the transportation and, despite the obstruction of his/her view, the positioning of a bulky object might be performed with a good level of precision.

3.2 Basic goal driven variable admittance control

In the proposed strategy, the admittance parameters are varied according to the direction of the human force and of the position of the target end-effector with respect to the one occupied by the robot.

Consequently, the space dependency of the filter parameters has been modelled with an ellipsoid, whose axes direction and length are of utter importance.

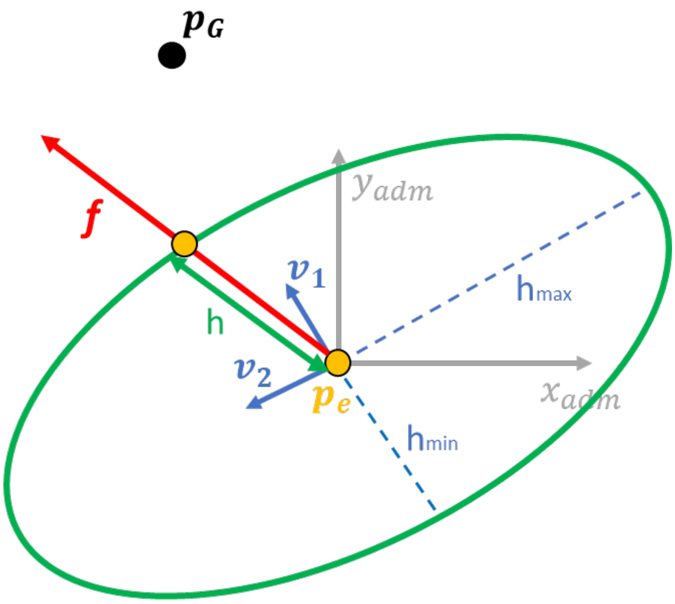

Figure 3.1: Representation of the ellipsoid that defines the parameters space dependency.

Taking an ellipsoid centred in the origin into account, this can be defined by a set of points $\boldsymbol{x} \in \mathbb{R}^3$ belonging to its surface, satisfying the following equation:

$$\dot{\boldsymbol{x}}^T \boldsymbol{A} \dot{\boldsymbol{x}} = 1 \tag{3.1}$$

where $\boldsymbol{A}$ is a 3x3 positive definite matrix describing the ellipsoid.

The eigenvectors $\boldsymbol{v_i}$, with $i = 1, 2, 3$, of matrix $\boldsymbol{A}$ are representative of the ellipsoid principal axes direction, chosen as follows:

- the direction of the first main axis, $\boldsymbol{v_1}$, is set coincident to the direction of the line connecting the actual position of the end-effector $\boldsymbol{p_e}$ with the goal position $\boldsymbol{p_G}$;
- the direction of $\boldsymbol{v_2}$ is set perpendicular to $\boldsymbol{v_1}$, in such a way that it belongs to an horizontal plane parallel to the ground;
- the direction of $\boldsymbol{v_3}$ is the result of a cross product between the directions of the two previous axes.

Along with the axes direction, their lengths have to be properly set.

The main axis $\boldsymbol{v_1}$ is the shortest one because it has to represent the minimum fatigue direction, *i.e.* the direction along which the virtual parameters of the admittance filter are set to the minimum.

Hence, if the worker applies a force along $\boldsymbol{v_1}$, he/she will be subjected to low effort. On the contrary, whenever the direction of the applied force deviates from the direction of the main axis, higher energy levels will be required to move the end-effector, reaching the maximum effort when the operator moves it along the direction of $\boldsymbol{v_2}$ and $\boldsymbol{v_3}$, *i.e.* in the plane normal to $\boldsymbol{v_1}$.

Therefore, the direction of the ellipsoid principal axes are expressed as:

$$\begin{cases} \boldsymbol{v_1} = \dfrac{\boldsymbol{p_G} - \boldsymbol{p_e}}{\|\boldsymbol{p_G} - \boldsymbol{p_e}\|} \\ \boldsymbol{v_2} = \dfrac{\boldsymbol{z} \times \boldsymbol{v_1}}{\|\boldsymbol{z} \times \boldsymbol{v_1}\|} \\ \boldsymbol{v_3} = \boldsymbol{v_1} \times \boldsymbol{v_2} \end{cases} \tag{3.2}$$

where $\boldsymbol{p_G}$ is the absolute goal position, $\boldsymbol{p_e}$ is the end-effector position and $\boldsymbol{z}$ is the unit vector pointing the z-direction of the ellipsoid reference frame, which is oriented as the global one. The eigenvectors can be arranged in a 3x3 matrix $\boldsymbol{Q}$:

$$\boldsymbol{Q} = [\boldsymbol{v_1}|\boldsymbol{v_2}|\boldsymbol{v_3}] \tag{3.3}$$

Since the 3-dimensional vectors constituting the matrix $\boldsymbol{Q}$ are representative of the spatial coordinates of the ellipsoid axes, $\boldsymbol{v_1}$, $\boldsymbol{v_2}$ and $\boldsymbol{v_3}$ (computed with Eq. 3.2), and then normalised, $\boldsymbol{Q}$ also expresses the orientation of the ellipsoid principal axes frame with respect to the frame of original definition (*i.e.* centred in correspondence of the robot basis). Being $\boldsymbol{Q}$ a rotation matrix, it is also an orthogonal matrix, *i.e.* its inverse is equal to its transpose ($\boldsymbol{Q}^{-1} = \boldsymbol{Q}^T$).

Furthermore, since in the considered admittance filter both the virtual mass and damping parameters must be changed, two ellipsoids, one for mass and one for damping, can be defined. They share the same axes directions and therefore they are represented by the same matrix $\mathbf{Q}$.

In the developed approach, the value of a given virtual parameter at a precise time instant is set equal to the distance between the ellipsoid centre and a point belonging to the ellipsoid surface, which is found by intersecting the ellipsoid itself with a line directed as the applied force. Therefore, a length corresponding to the minimum value the virtual parameters can take is assigned to the first semi-axis (which corresponds to the minimum effort direction), while the remaining two are associated to a length equal to the maximum value of the aforementioned parameters.

The eigenvalues λ_i of $\boldsymbol{A}$, with i = 1, 2, 3, are computed as the reciprocals of the squares of the semi-axes length. Therefore, for a generic parameter h, representing the value to be assigned to the virtual mass or damping and characterised by a minimum and a maximum values, h_{min} and h_{max} respectively, the associated eigenvalues are selected as:

$$\begin{cases} \lambda_1 = \dfrac{1}{(h_{min})^2} \\ \lambda_2 = \dfrac{1}{(h_{max})^2} \\ \lambda_3 = \dfrac{1}{(h_{max})^2} \end{cases} \tag{3.4}$$

The eigenvalues can be collected inside a 3x3 diagonal matrix $\boldsymbol{\Lambda_h}$.

It follows that the matrix $\boldsymbol{A_h}$, representing the ellipsoid, can be obtained as:

$$\boldsymbol{A_h} = \boldsymbol{Q}\Lambda_{\boldsymbol{h}}\boldsymbol{Q}^{-1} = \boldsymbol{Q}\Lambda_{\boldsymbol{h}}\boldsymbol{Q}^{T} \tag{3.5}$$

Hence, the ellipsoid representing the virtual mass, $\boldsymbol{A_m}$, and the one representing the damping, $\boldsymbol{A_d}$, will be computed according to the minimum and the maximum values of the mass and damping parameters respectively, retrieving the length of each ellipsoid main axis.

The value of the generic parameter h is calculated as the distance between the centre of the ellipsoid and one of the two points resulting from the intersection between its shape and a straight line directed as the human force vector $\boldsymbol{f}$. Such a value can be found through the following formula:

$$h = \frac{1}{\sqrt{\boldsymbol{u_f}^T \boldsymbol{A_h} \boldsymbol{u_f}}} \tag{3.6}$$

where $\boldsymbol{u_f}$ is a unit vector directed as the force $\boldsymbol{f}$, while h corresponds to the value to be assigned to the virtual mass or damping and takes into account the relative direction of the applied force with respect to the goal position.

In Fig. 3.1 a top view representation of the 3-dimensional ellipsoid (projected to an ellipse) is reported: it is defined in a frame centred in the end-effector and oriented as the global one. It is possible to observe that $\boldsymbol{v_1}$ is pointing towards the goal position and, along this direction, the length of the semi-axis is the shortest one.

Instead, Fig. 3.2 depicts a top view of the ellipsoid (still centered in $\boldsymbol{p_e}$) when the end-effector position is changed along a semi-circular trajectory. Notice that $\boldsymbol{v_1}$ (*i.e.* the minimum fatigue direction) always points towards the goal position $\boldsymbol{p_G}$. The integration of this method with any of the variable admittance strategy available in literature would be rather simple: it would just require the application of a transformation to the results of Eq. 3.6, taking into account the scaling of virtual parameters based on acceleration, cruise speed and deceleration states.

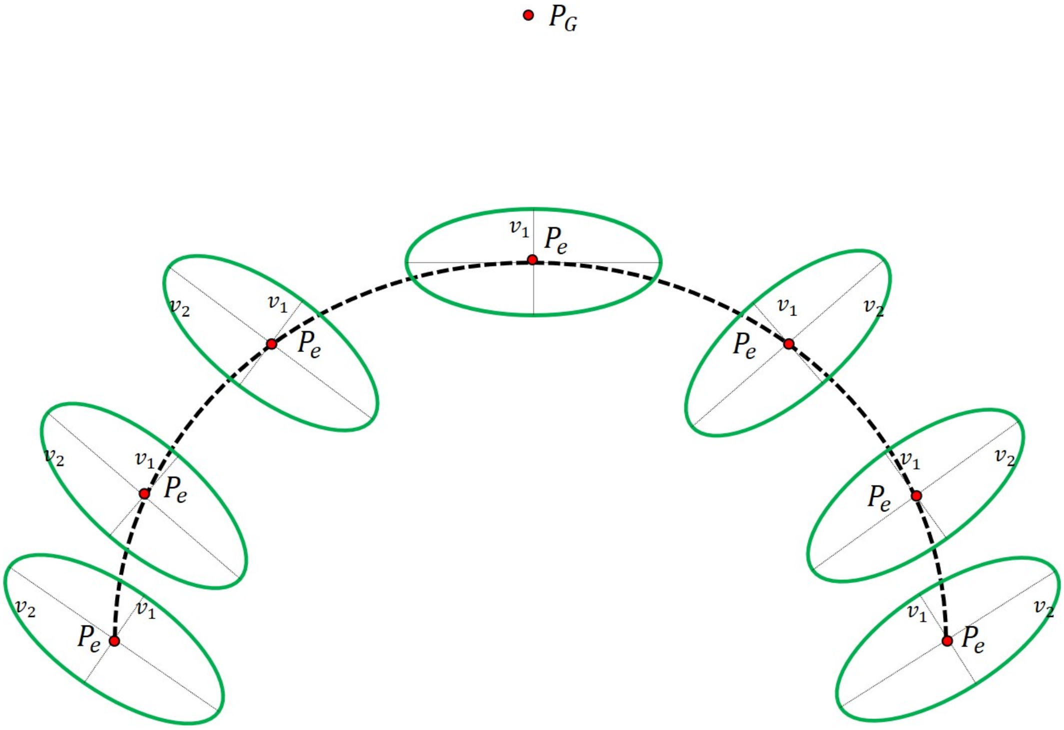

Figure 3.2: High view - corresponding to a 2-dimensional analysis - schematised representation of the variation of the first principal axis of the ellipsoid, $\boldsymbol{v_1}$, when the relative position between $\boldsymbol{p_e}$ and $\boldsymbol{p_G}$ is changed

In the following, two improvements to the aforementioned strategy will be discussed.

3.3 Damping ellipsoid

According to literature, a low mass is desirable both in the acceleration phase, when the human force is pointing to the goal, and in the deceleration one, when the human force is pointing in a direction opposite to the target position. This behavior is guaranteed by the symmetric structure of the mass ellipsoid, $\boldsymbol{A_m}$. On the contrary, low damping is advisable when the human is pushing towards the target, while high damping is convenient when the worker is pulling the robot to brake in the proximity of the goal position. In this way the operator will be helped in slowing the manipulator down.

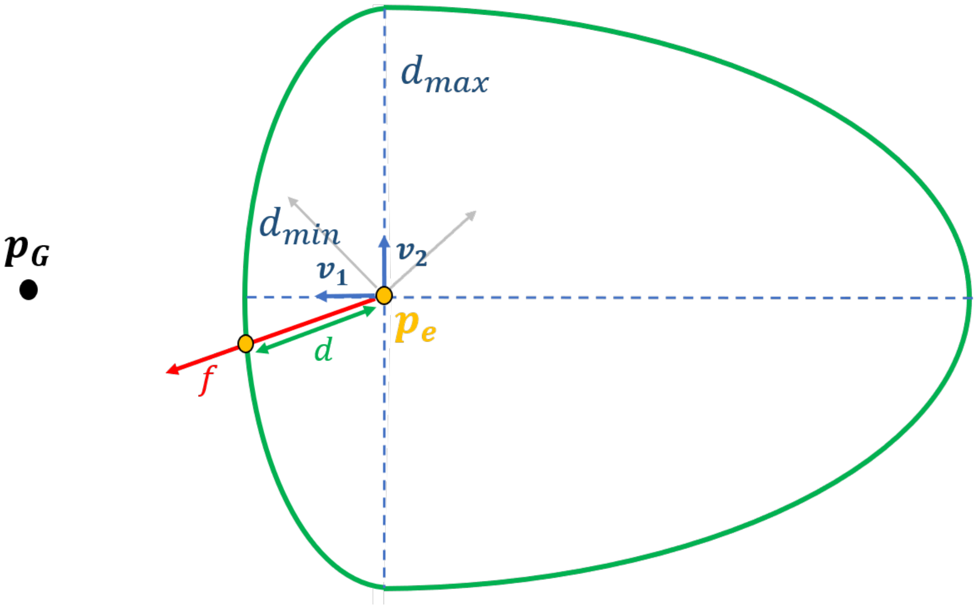

Figure 3.3: Representation of the improved shape for the damping constituted by the union of two half-ellipsoids.

However, to obtain this result, the ellipsoid $\boldsymbol{A_d}$ describing the damping parameter has to be defined in a different way from the one described in Sec. 3.2. In fact, considering a plane described by its second and the third axes and normal to $\boldsymbol{v_1}$, the main idea consists in dividing the damping ellipsoid into two half-spaces, identified by such plane. In particular, two different half-ellipsoids corresponding to the above-mentioned plane are combined: one corresponds to half of the ellipsoid previously described, belonging to the half-space containing the target; concerning the second half, its orientation is defined by $\boldsymbol{v_1}$, $\boldsymbol{v_2}$ and $\boldsymbol{v_3}$, while the length of the first semi-axis can be set either greater or equal to the maximum length of the other two.

It is worth to mention that, since in literature no limitation is imposed to the maximum value assignable to mass/damping parameters, in the present framework the term "maximum" does not represent a real physical limit, but it is a value arbitrarily chosen. In this way, the damping parameter is described by an asymmetric spatial shape with no discontinuity (Fig. 3.3).

3.4 Ellipsoid first principal axis direction

In the previous sections, the minimum effort direction (*i.e.* the direction of the first principal axis $\boldsymbol{v_1}$) was selected coincident to the one of the straight lines connecting the actual end-effector position $\boldsymbol{p_e}$ and the goal one $\boldsymbol{p_G}$. However, this would not be the best solution if, for some reason, the actual speed direction did not point towards the target, *e.g.* in case of a curvilinear path. In fact, in such a case, the choice previously made would induce an additional effort for the human since, in order to change the speed direction, he/she will apply a continuous directional force profile not instantaneously directed as $\boldsymbol{v_1}$, thus entailing a high damping value and leading to a large human fatigue. In order to avoid these undesired effects, a better solution is that the human progressively redirects to the target along a curve in a smooth way.

In literature, a widely adopted strategy to smoothly connect the actual position to the goal one is represented by the **minimum curvature path**. In the frame of the current work, such strategy was implemented in order to overcome the issues previously described.

3.4.1 Minimum Curvature path

To reproduce the ideal reaching path of the human hand in the most realistic way, a **minimum curvature path** [25] was selected.

As it will be further explained, since this path is obtained minimizing the integral of a certain function over a given temporal or spatial horizon, a time-based method appears to be unsuitable, since it would force the imposition of a limit on the duration of each reaching motion. As a consequence, the applicability of the algorithm would be restricted to a small set of possibilities, making it not consistent with the purpose of collaborative operation.

On the contrary, the main focus of the developed algorithm is to impose that, during the collaborative task, the path followed by the human operator will lead him/her to reach a prescribed target position placed into the operating space regardless of the time needed to reach the goal.

To obtain this result, the path $\boldsymbol{p}$ will be parameterised with respect to the natural coordinate $s \in (0,1)$:

$$\boldsymbol{p} = \boldsymbol{p}(s) \tag{3.7}$$

The desired *minimum curvature path* $\boldsymbol{p}(s)$ is associated with a polynomial structure of the 4th-order, since it has to satisfy four different constraints imposed on the initial and final position, and the initial and final velocity. Moreover, $\boldsymbol{p}(s)$ has to minimize the following cost function:

$$\boldsymbol{J_{MinCurv}} = \int_0^1 \boldsymbol{p}(s)''^T \boldsymbol{p}(s)'' ds \tag{3.8}$$

where $\boldsymbol{p}(s)''$ represents the second derivative of the end-effector position with respect to the natural coordinate s, $\frac{\partial^2 \boldsymbol{p}}{\partial s^2}$.

In order to reproduce the constraints of the actual human motion from a generic initial point to the target position, the following boundary conditions were introduced:

- $\boldsymbol{p}(s=0) = \boldsymbol{p_e(k)}$
- $\boldsymbol{p}'(s=0) = \boldsymbol{\dot{p}_e(k)}$
- $\boldsymbol{p}(s=1) = \boldsymbol{p_G}$
- $\boldsymbol{p}'(s=1) = \mathbf{0}$

where $\boldsymbol{p}'(s)$ denotes the first derivative of the path $\boldsymbol{p}(s)$ with respect to s, $\frac{\partial \boldsymbol{p}}{\partial s}$, $\boldsymbol{p_e(k)}$ and $\boldsymbol{\dot{p}_e(k)}$ are the actual position and speed of the end-effector respectively, and $\boldsymbol{p_G}$ represents the goal position. In particular:

- At time k the path must start in the current end-effector position, indicated as $\boldsymbol{p_e(k)}$;
- At time k the path must start with the current end-effector speed, indicated as $\boldsymbol{\dot{p}_e(k)}$;
- the path must end in correspondence of the considered target position $\boldsymbol{p_G}$;
- the path must arrive with zero velocity at the target position.

Once the constraints are defined, a fourth order polynomial (Eq. 3.9) representing the desired path is used to solve the optimization problem, minimizing the objective function defined in Eq. 3.8 and satisfying the aforementioned constraints:

$$\boldsymbol{p}(s) = \boldsymbol{a_0} + \boldsymbol{a_1} s + \boldsymbol{a_2} s^2 + \boldsymbol{a_3} s^3 + \boldsymbol{a_4} s^4 \tag{3.9}$$

Hereafter, the coefficients of the polynomial are introduced into a vector $\boldsymbol{C^*}$, reported below:

$$\boldsymbol{C^*} = \begin{bmatrix} \boldsymbol{a_0} \\ \boldsymbol{a_1} \\ \boldsymbol{a_2} \\ \boldsymbol{a_3} \\ \boldsymbol{a_4} \end{bmatrix} \tag{3.10}$$

The **Lagrange multipliers** method is then used to solve the constrained optimization problem. This strategy is generally applied to find the local maxima and minima of a function, in this case represented by $\boldsymbol{J_{MinCurv}}$, which is subjected to equality constraints, *i.e.* $g(\boldsymbol{C}*) = 0$.

Using this procedure, it is possible to solve the optimization problem minimizing the so-called **Lagrangian expression**:

$$\boldsymbol{J^*_{MinCurv}}(\boldsymbol{C^*}, \lambda) = \boldsymbol{J_{MinCurv}}(\boldsymbol{C^*}) - \boldsymbol{\lambda} g(\boldsymbol{C^*}) \tag{3.11}$$

In the following, the whole procedure to solve the constrained optimization problem, exploiting the aforementioned Lagrangian expression, is described.

Eq. 3.12 represents the first order partial derivative:

$$\boldsymbol{p}'(s) = \boldsymbol{a_1} + 2\boldsymbol{a_2}s + 3\boldsymbol{a_3}s^2 + 4\boldsymbol{a_4}s^3 \tag{3.12}$$

while Eq. 3.13 is the second order partial derivative:

$$\boldsymbol{p}''(s) = 2\boldsymbol{a_2} + 6\boldsymbol{a_3}s + 12\boldsymbol{a_4}s^2 \tag{3.13}$$

Then, substituting the set of initial conditions into $\boldsymbol{p}(0)$ and $\boldsymbol{p}'(0)$, it is possible to retrieve the trivial expressions for the polynomial coefficients $\boldsymbol{a_0}$ and $\boldsymbol{a_1}$:

- $\boldsymbol{a_0} = \boldsymbol{p_e(k)}$
- $\boldsymbol{a_1} = \boldsymbol{\dot{p}_e(k)}$

Substituting the expressions of $\boldsymbol{a_0}$ and $\boldsymbol{a_1}$ into $\boldsymbol{J_{MinCurv}}$, the latter can be rewritten as:

$$\boldsymbol{J_{MinCurv}} = \int_0^1 \left(\begin{bmatrix} 2\boldsymbol{a_2} & 6\boldsymbol{a_3} & 12\boldsymbol{a_4} \end{bmatrix} \begin{bmatrix} 1 \\ s \\ s^2 \end{bmatrix} \begin{bmatrix} 1 & s & s^2 \end{bmatrix} \begin{bmatrix} 2\boldsymbol{a_2} \\ 6\boldsymbol{a_3} \\ 12\boldsymbol{a_4} \end{bmatrix} \right) ds \tag{3.14}$$

Furthermore, denoting with:

$$\boldsymbol{C} = \begin{bmatrix} 2\boldsymbol{a_2} \\ 6\boldsymbol{a_3} \\ 12\boldsymbol{a_4} \end{bmatrix} \tag{3.15}$$

and

$$\boldsymbol{\beta} = \begin{bmatrix} 1 & \frac{1}{2} & \frac{1}{3} \\ \frac{1}{2} & \frac{1}{3} & \frac{1}{4} \\ \frac{1}{3} & \frac{1}{4} & \frac{1}{5} \end{bmatrix} \tag{3.16}$$

Eq. 3.14 can be written in a more convenient and synthetic way:

$$\boldsymbol{J_{MinCurv}} = \boldsymbol{C}^T \boldsymbol{\beta} \boldsymbol{C} \tag{3.17}$$

At this point, the so-called *homogeneous constraint equations* are computed substituting the expressions of $\boldsymbol{a_0}$ and $\boldsymbol{a_1}$ into the ones of $\boldsymbol{p(s)}$ and $\boldsymbol{p'(s)}$, keeping $s = 1$:

$$\begin{bmatrix} 1 & 1 & 1 \end{bmatrix} \begin{bmatrix} \boldsymbol{a_2} \\ \boldsymbol{a_3} \\ \boldsymbol{a_4} \end{bmatrix} - (\boldsymbol{p_G} - \boldsymbol{p_e(k)} - \boldsymbol{\dot{p}_e(k)} = 0 \tag{3.18}$$

$$\begin{bmatrix} 2 & 3 & 4 \end{bmatrix} \begin{bmatrix} \boldsymbol{a_2} \\ \boldsymbol{a_3} \\ \boldsymbol{a_4} \end{bmatrix} - (-\boldsymbol{\dot{p}_e(k)}) = 0 \tag{3.19}$$

Then, defining:

$$\boldsymbol{E} = \begin{bmatrix} 1 & 1 & 1 \\ 2 & 3 & 4 \end{bmatrix} \tag{3.20}$$

and

$$\boldsymbol{\alpha} = \begin{bmatrix} \boldsymbol{p_G} - \boldsymbol{p_e}(\boldsymbol{k}) - \dot{\boldsymbol{p}}_{\boldsymbol{e}}^{\boldsymbol{k}} \\ -\dot{\boldsymbol{p}}_{\boldsymbol{e}}(\boldsymbol{k}) \end{bmatrix} \tag{3.21}$$

the Lagrangian expression $\boldsymbol{J^*_{MinCurv}}$ is retrieved:

$$\boldsymbol{J^*_{MinCurv}} = \boldsymbol{C}^T \boldsymbol{\beta} \boldsymbol{C} + \boldsymbol{\lambda}^T (\boldsymbol{E}\boldsymbol{C}^* - \boldsymbol{\alpha}) \tag{3.22}$$

where $\boldsymbol{\lambda}$ corresponds to the column vector $\begin{bmatrix} \lambda_1 \\ \lambda_2 \end{bmatrix}$ and:

$$\boldsymbol{C} = \begin{bmatrix} 2 & 0 & 0 \\ 0 & 6 & 0 \\ 0 & 0 & 12 \end{bmatrix} \boldsymbol{C}^* \tag{3.23}$$

In order to find the expression of the coefficients $\boldsymbol{a_2}$, $\boldsymbol{a_3}$ and $\boldsymbol{a_4}$, the following system of equations has to be solved:

$$\begin{cases} \frac{\partial (J^*(\boldsymbol{a_2},\boldsymbol{a_3},\boldsymbol{a_4},\lambda_1,\lambda_2))^T}{\partial \boldsymbol{a_2}} = 0 \\ \frac{\partial (J^*(\boldsymbol{a_2},\boldsymbol{a_3},\boldsymbol{a_4},\lambda_1,\lambda_2))^T}{\partial \boldsymbol{a_3}} = 0 \\ \frac{\partial (J^*(\boldsymbol{a_2},\boldsymbol{a_3},\boldsymbol{a_4},\lambda_1,\lambda_2))^T}{\partial \boldsymbol{a_4}} = 0 \\ \frac{\partial (J^*(\boldsymbol{a_2},\boldsymbol{a_3},\boldsymbol{a_4},\lambda_1,\lambda_2))^T}{\partial \lambda_1} = 0 \\ \frac{\partial (J^*(\boldsymbol{a_2},\boldsymbol{a_3},\boldsymbol{a_4},\lambda_1,\lambda_2))^T}{\partial \lambda_2} = 0 \end{cases} \tag{3.24}$$

Eventually, the formulation of the coefficients constituting the fourth order polynomial, describing the minimum curvature path, is:

$$\boldsymbol{a_0} = \boldsymbol{p_e}(\boldsymbol{k}) \tag{3.25}$$

$$\boldsymbol{a_1} = \dot{\boldsymbol{p}}_{\boldsymbol{e}}(\boldsymbol{k}) \tag{3.26}$$

$$\boldsymbol{a_2} = 3\boldsymbol{p_G} - 3\boldsymbol{p_e}(\boldsymbol{k}) - 2\dot{\boldsymbol{p}}_{\boldsymbol{e}}(\boldsymbol{k}) \tag{3.27}$$

$$\boldsymbol{a_3} = -(2\boldsymbol{p_G} - 2\boldsymbol{p_e}(\boldsymbol{k}) - \dot{\boldsymbol{p}}_{\boldsymbol{e}}(\boldsymbol{k}) \tag{3.28}$$

$$\boldsymbol{a_4} = \boldsymbol{0}; \tag{3.29}$$

3.4.2 Minimum curvature path integration into the developed algorithm

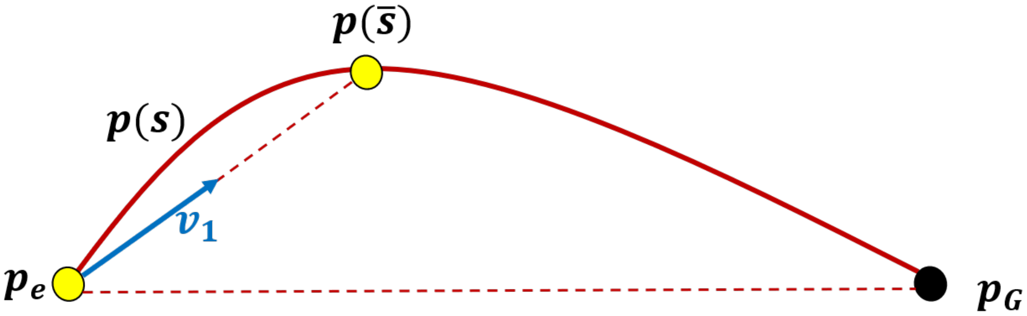

Figure 3.4: Representation of the minimum curvature path and of the new ellipsoid first semi-axis direction.

Once the parameters of the fourth-order polynomial are found, the minimum curvature path $\boldsymbol{p}(s)$, expressed in the normalized coordinate s, is identified. It represents the minimum curved path connecting the actual position of the end-effector to the goal one, satisfying the constraints imposed on both the actual and final positions and velocities of the manipulator end-effector.

At this point, the direction of the ellipsoid principal axis must be found. In particular, as can be noted from figure 3.4, considering that $s \in (0,1)$ and taking into account a point $\boldsymbol{p}(\bar{s})$ along the path, the direction of $\boldsymbol{v_1}$ is selected as:

$$\boldsymbol{v_1} = \frac{\boldsymbol{p}(\bar{s}) - \boldsymbol{p_e}}{||\boldsymbol{p}(\bar{s}) - \boldsymbol{p_e}||} \tag{3.30}$$

while the directions associated to the remaining two principal axes are computed as in Eq. 3.2.

The choice of different values of $\bar{s}$ will influence the direction of $\boldsymbol{v_1}$. If $\bar{s}$ is set equal to 1, then the principal axes directions become again equal to the ones defined by Eq. 3.2, so that the described minimum curvature approach can be considered as an additional generalization of the strategy initially proposed.

On the contrary, if $\bar{s}$ is chosen equal to 0, then the main axis is directed as the actual speed, thus the goal position would not be considered and the strategy would completely accommodate whatever motion the robot is performing, providing no assistance to the operator in redirecting to the desired target.

Therefore a value of $\bar{s}$, included in its definition range, must be selected to help the human moving more fluidly than he/she would do if the strategy presented in Sec. 3.2 was adopted.

Usually it is desirable to have a greater freedom of motion at the beginning of the movement, while a more precise and constrained motion is desirable at the end of the path, when the human is approaching towards the target position.

Therefore, it was decided not to set a fixed value for $\bar{s}$, but to change it according to the following equation:

$$\bar{s} = 1 - e^{-\frac{\|\boldsymbol{p_e} - \boldsymbol{p_0}\|}{\|\boldsymbol{p_e} - \boldsymbol{p_G}\|}} \tag{3.31}$$

where $\boldsymbol{p_e}$ is the actual end-effector position, $\boldsymbol{p_G}$ is the goal position and $\boldsymbol{p_0}$ is the starting point of the whole motion.

In this way, at the beginning of the motion, when $\boldsymbol{p_e}$ is coincident with $\boldsymbol{p_0}$, $\bar{s}$ will be equal to zero and the human motion will thus be completely free. On the other hand, when the human will move towards the goal, $\bar{s}$ will increase until it reaches 1 in correspondence of the goal position, allowing, in this way, a progressively low freedom of motion.

3.5 Quadratic constraint optimization problem

In the previous Section, the procedure adopted to select the direction of the first principal axis $\boldsymbol{v_1}$ of the ellipsoid was described. However, it may happen that the operator could move the end-effector of the manipulator towards areas out of the operating space, causing the robot to enter an error state due to both joint limitations and its mechanical structure. Indeed, any industrial manipulator is subjected to restrictions imposed on the joints maximum/minimum displacements and velocities. These limits, expressed in [deg] and in [deg/s] respectively, referred to the ABB IRB140, *i.e.* the robot used in the experimental tests, are summarized in the following table:

Joint	q_{inf}	q_{sup}	$\dot{q}_{max}$
1	-180	180	200
2	-110	90	200
3	-50	230	260
4	-200	200	360
5	-115	115	360
6	-400	400	450

Table 3.1: ABB IRB140 joints limits in minimum and maximum allowed displacements and in maximum velocities

Besides, the constitutional limits proper of the robot generate constraints within the operating space, defining areas where the operator should not carry the end-effector to avoid fault states, such as the singularities of the manipulator. In order to satisfy these constraints, the procedure described in Sec. 3.4.2 has also to include the resolution of a **quadratic constrained optimisation problem**, whose main objective is to find the direction to be assigned to $\boldsymbol{v_1}$, so to be as close as possible to the one computed in Sec. 3.4.2.

The resolution of the quadratic constrained optimisation problem is based on the exploitation of a reactive approach, which only considers the area surrounding the end-effector, the constraints proper of the work-space and the limits imposed to the minimum and maximum joints displacements and velocities.

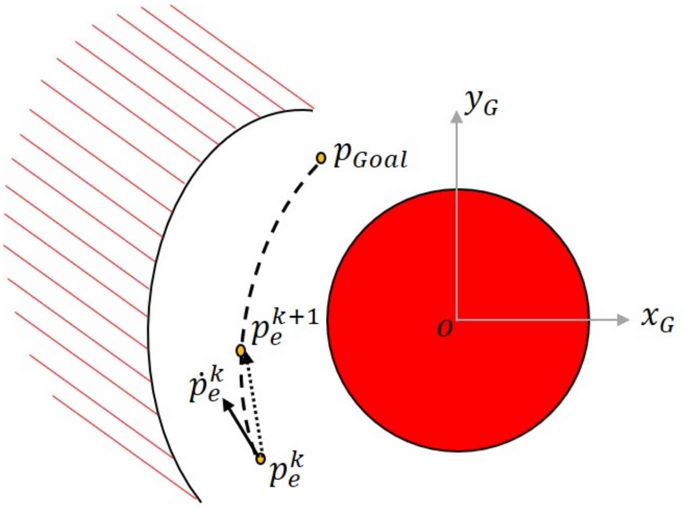

Figure 3.5: Representation of the operating space with some of the considered constraints, generating a forbidden area, represented in red. The end-effector of the manipulator must not enter into the red zones (both dashed and not) to not go into a failure state.

The resolution of such problem was based on the exploitation of the *fmincon* Matlab function, a non-linear programming solver that finds the minimum of a problem, which is specified as:

$$\min_{\boldsymbol{x}} f(\boldsymbol{x}) such that := \begin{cases} \boldsymbol{c}(\boldsymbol{x}) \leq 0 \\ \boldsymbol{c_{eq}}(\boldsymbol{x}) = 0 \\ \boldsymbol{A x} \leq \boldsymbol{b} \\ \boldsymbol{A_{eq} x} = \boldsymbol{b_{eq}} \\ \boldsymbol{l_b} \leq \boldsymbol{x} \leq \boldsymbol{u_b} \end{cases}$$

where $\boldsymbol{b}$ and $\boldsymbol{b_{eq}}$ are vectors, $\boldsymbol{A}$ and $\boldsymbol{A_{eq}}$ are matrices, $\boldsymbol{c}(\boldsymbol{x})$ and $\boldsymbol{c_{eq}}$ are functions that return vectors, and $f(\boldsymbol{x})$, is the cost function to be minimized.
For the problem at hand, consider that:

- $\boldsymbol{\Delta x} = \boldsymbol{J\Delta q}$, where $\boldsymbol{\Delta x}$ corresponds to the variation of the Cartesian end-effector position, $\boldsymbol{J}$ is the Jacobian matrix and $\boldsymbol{\Delta q}$ corresponds to the variation of the joint position;

- two vectors are aligned *if and only if* their vector product is equal to zero and, at the same time, their scalar product is greater than zero.

The form of the implemented fmincon function, in the specific case of application, is defined as:

$$\min_{\boldsymbol{\Delta q}} \|((\boldsymbol{J\Delta q}) \wedge \boldsymbol{\Delta x_{ref}})\| := \begin{cases} \boldsymbol{c}(\boldsymbol{\Delta q}) \leq 0 \\ -\Delta \boldsymbol{x_{ref}^{T}}(\boldsymbol{J\Delta q}) \leq 0 \\ \boldsymbol{q_{min}} \leq \boldsymbol{\Delta q} + \boldsymbol{q} \leq \boldsymbol{q_{max}} \end{cases}$$

where $\boldsymbol{\Delta x_{ref}}$ represents the direction of the first axis of the ellipsoid computed with the minimum curvature path procedure described in Sec. 3.4.2, while $\boldsymbol{J\Delta q}$ corresponds to $\boldsymbol{\Delta x}$, *i.e.* the new direction of $\boldsymbol{v_1}$. Minimising the vector product between $\boldsymbol{J\Delta q}$ and $\boldsymbol{\Delta x_{ref}}$ with respect to $\boldsymbol{\Delta q}$, it was possible to find the $\boldsymbol{\Delta x}$ as more aligned as possible to $\boldsymbol{\Delta x_{ref}}$, satisfying at the same time the imposed constraints. The output of the optimization problem is $\boldsymbol{\Delta q}$, which is then used to compute $\boldsymbol{\Delta x}$ as follows:

$$\boldsymbol{J\Delta q} = \boldsymbol{\Delta x} \tag{3.32}$$

$\boldsymbol{\Delta x}$ is eventually normalised for its own norm, obtaining a unit vector in Cartesian coordinates that represents the new direction of $\boldsymbol{v_1}$.

Chapter 4

Experimental results

4.1 Introduction

In order to validate the developed algorithm, two sets of experiments were performed involving ten volunteers.

In the first one, the developed approach (**VAF**: variable admittance filter) is compared with three invariant admittance controls, whose parameters were set to low (**IAF-L**), medium (**IAF-M**) and high (**IAF-H**) values respectively. For all these techniques, the parameters were tuned to obtain the same bandwidth, providing the operator with a more natural feeling during the manual guidance. Moreover, the operator had the task to reach, as quickly as possible, a certain predefined marked goal position, trying to ensure a good level of precision. The target position was selected in order to make it unreachable by following a linear path, forcing the operator to move along a path characterised by a certain curvature radius. Hereafter, the obtained results were analyzed in terms of *task execution time*, *positioning accuracy*, *path length* and *energy* required to the operator to complete the operation.

In the second set of experiments, instead, the operator was asked to reach a goal whose position, selected within the robot operating space, was unknown, since it was randomly selected and not marked on the floor. Therefore, the main objective was to show the effectiveness of the proposed approach in providing the worker with a natural and intuitive directional feedback that would allow him/her to achieve the goal position with a certain precision, even if it could not be directly seen. This feature is of particular importance when the operator is transporting a bulky object: due to the size of the load, his/her sight could be obstructed. Thanks to the developed algorithm, the operator could reach the goal simply following the direction perceived as the one with "minor fatigue".

4.2 Experimental set-up

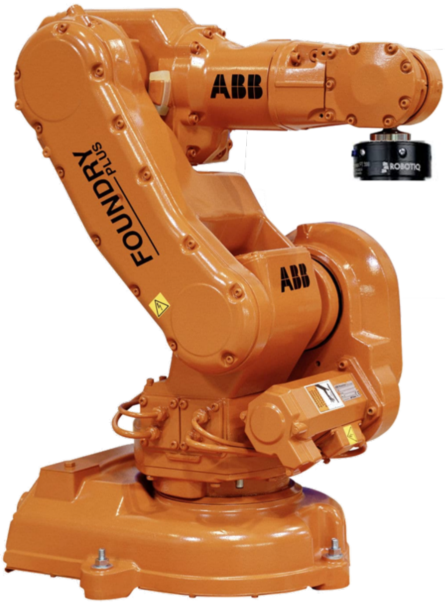

Figure 4.1: IRB 140 manipulator equipped with a 6 axis Robotiq FT300 F/T sensor

During the experimental campaign, the proposed control algorithm was tested in a setup including an ABB IRB 140 industrial robot, equipped with a 6 axis Robotiq FT300 F/T sensor, which is depicted in Fig. 4.1.

The robot is characterised by 6 degrees of freedom, has a capacity load of 6 Kg, a scope of 810 mm and weighs 98 Kg.
Thanks to its robust design, it can be mounted on the floor, on the ceiling, upside down, or on a wall, at any angle of inclination, as shown in Fig. 4.2.

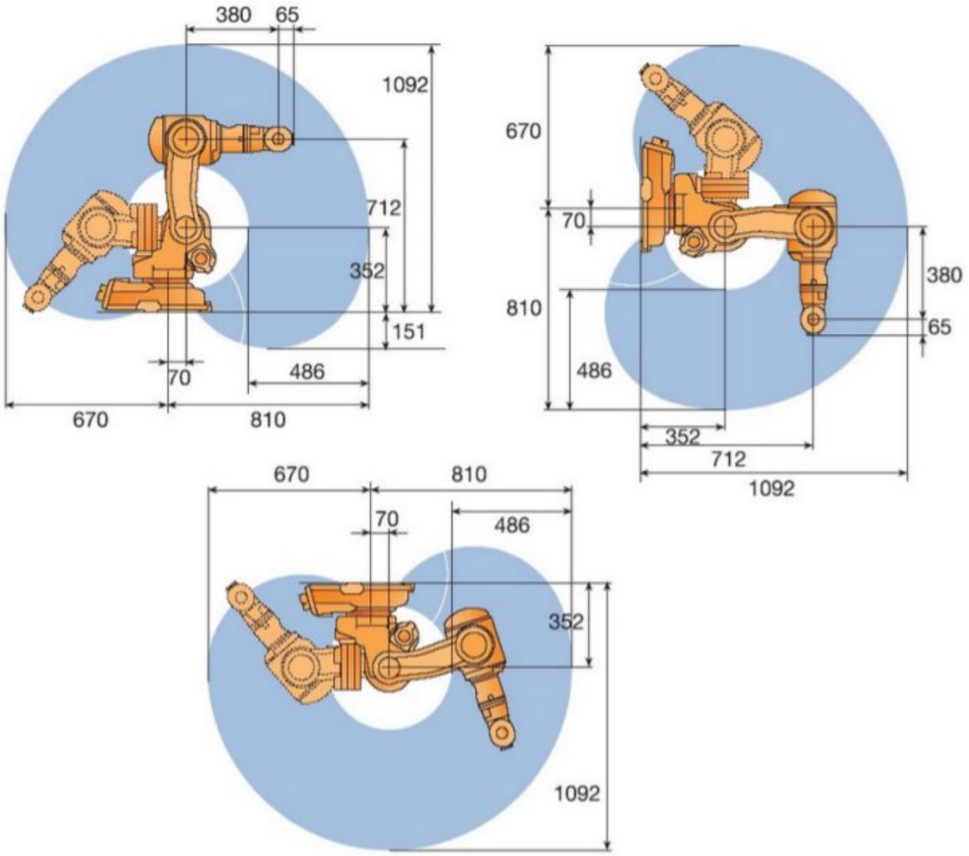
380
65
1092
712
352
151
70
486
670
810
670
70
810
486
380
65
352
712
1092
670
810
70
486
352
1092

Figure 4.2: Workspace of ABB IRB-140 robot.

Besides, it is equipped with integrated wiring, which makes it quite flexible, adaptable and easy to be integrated into any robotic process.

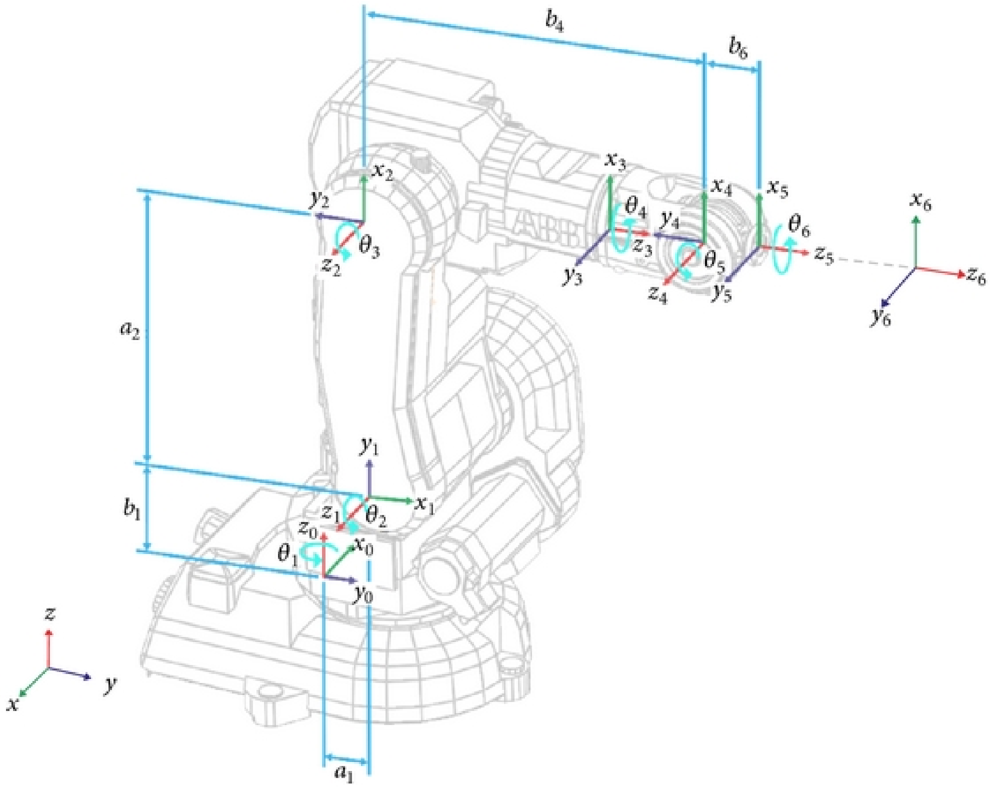
b_4
b_6
x_2
y_2
θ_3
z_2
x_3
θ_4
y_4
z_3
y_3
x_4
x_5
θ_6
z_5
θ_5
z_4
y_5
x_6
z_6
y_6
a_2
y_1
b_1
z_1
θ_2
x_1
z_0
x_0
θ_1
y_0
z
y
x
a_1

Figure 4.3: Architecture of the industrial robot IRB 140.

Joint	a_i	b_i	α_i	θ_i
1	70	352	$-\Pi/2$	θ_1
2	360	0	0	$\theta_2-\Pi/2$
3	0	0	$\Pi/2$	$\theta_3+\Pi$
4	0	380	$-\Pi/2$	θ_4
5	0	0	$\Pi/2$	θ_5
6	0	65	$\Pi/2$	$\theta_6-\Pi/2$

Table 4.1: D-H parameters for the robot.

The architecture of the IRB 140 [1] is shown in Fig. 4.3, where x_i, y_i and z_i are representative of the axis related to the frames attached to each link, while the **Denavit-Hartenberg** parameters are tabulated and summarized in Table 4.1:

- α_i is the angle around the axis x_i, defined between the axes z_{i-1} and z_i and taken as positive counter clockwise;
- θ_i is the angle around the axis z_{i-1}, defined between the axes x_{i-1} and x_i and taken as positive counter clockwise; in particular, it is the angular position of each joint.

All technical specifications, documents, CAD models and videos related to the aforementioned manipulator are available in [1].
The ABB IRB140 is endowed with an IRC5 control unit (Fig. 4.4), which was connected via Ethernet to an external PC running under a Linux operating system [11].

Figure 4.4: IRC 5 - Robot control unit

It allows hard real-time operations, obtaining an open controller configuration of the robot, where the PC serves as external control. Indeed, thanks to the exploitation of an interface, it was possible to conceptually insert the external PC between the IRC5 high-level control, generating the joint references, and the IRC5 low-level control, which receives the high-level references and produces the motors ones. Therefore, the desired reference were computed on the external PC and fed as input to the low-level control. In particular, the desired control strategy was developed using a Simulink GUI and then converted into an executable code through the Simulink Real-Time Workshop.

Exploiting the open control interface, the executable code runs in real-time dialogue with the IRC5 controller with a frequency of 250 Hz, feeding the joint references, computed by the external PC, to the low-level control. Indeed, the robot is already equipped with a position and speed controller for each joint, whose sampling time is 4 ms.

A handle was attached in correspondence of the end-effector attachment point, where the force sensor was mounted. Since only a positional admittance control has been implemented, the handle keeps its orientation for the entire duration of the movement.

Moreover, the human applies a force at the handle and the manipulator moves in the 3-dimensional Cartesian work-space according to the corresponding end-effector speed reference, generated by the admittance filter, which is then converted in joints position and velocity references. In addition, since the target point for both sets of experiments laid in the horizontal plane, it was possible to think of the target as a vertical line passing through the goal, placed in any horizontal plane independently from the height of the end-effector (red line in Fig. 4.5).

The decision to neglect the height of the target mainly derives from the difficulties that the operator would have encountered in precisely identifying the target position if the goal had been imposed in the 3-dimensional space, but also from the complications that would have arisen in evaluating performances.

Therefore, to be consistent with the aforementioned experimental set-up, the ellipsoid defined in the 3-dimensional space (Sec. 3.2) was replaced by an ellipse in the horizontal plane. As a consequence, in all the experiments an invariable admittance filter with constant parameters along the z-axis was adopted, while different techniques in the horizontal plane were applied.

Before carrying out the experiments, some empirical tests were performed so to define the minimum value which could be assigned to the virtual parameters of the admittance filter for stability purposes. Since, according to literature, the minimum value to be assigned to the virtual mass is $6 \div 10$ times lower than the real one [19], it was set as equal to 10 kg. Then, keeping the value of the virtual mass fixed to its minimum, the lowest possible value for the damping was selected in order to avoid any robot oscillations in case of highly stiff human arm. To do so, the operator was asked to move the end-effector of the manipulator while the virtual mass was kept constant at its minimum and the virtual damping parameter was progressively reduced. As a result of these experimental tests, it was found that the minimum admissible value for the virtual damping parameter was equal to 100 $\frac{Ns}{m}$.

4.3 First test: objectives, set-up and outcomes

In the first set of experiments, each volunteer was asked to move the end-effector of the robot from the starting position to the target one, repeating the process for 5 times and trying to be as quick and precise as possible. In order to make the goal position visible for the operator, the corresponding point was marked on the ground; a laser was mounted at the tip of the handle, pointing downwards, to show the operator the relative position of the end-effector with respect to the final one, thus eliminating any possible evaluation error due to his/her prospective.

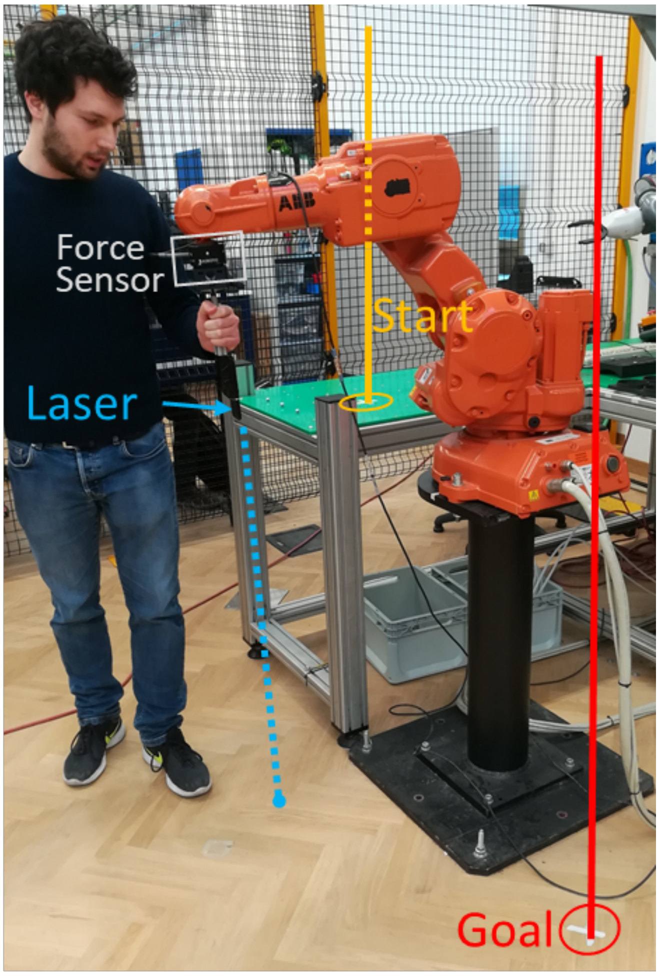

Figure 4.5: Picture of the experimental set-up for the first set of experiments.

During the execution of this first set of experiments, each volunteer was asked to try all the following four techniques, in a random order:

1. **Invariable admittance filter** with low damping (**IAF-L**):
    - d = 100 $\frac{Ns}{m}$
    - m = 10 kg
2. **Invariable admittance filter** with medium damping (**IAF-M**):
    - d = 250 $\frac{Ns}{m}$
    - m = 25 kg
3. **Invariable admittance filter** with high damping (**IAF-H**):
    - d = 400 $\frac{Ns}{m}$
    - m = 40 kg
4. **Variable admittance filter** with the damping parameter computed by implementing the developed technique, with all the discussed improvements, while the virtual mass parameter is chosen so as to keep the bandwidth of the filter always equal to 10 $\frac{rad}{s}$ (**VAF**).

Note that the virtual damping and mass used in both the invariant admittance filters and the variable one were chosen in such a way that the bandwidth was always equal to 10 $\frac{rad}{s}$, thus making the collaboration more intuitive for the operators.

The main objective of this first set of experiments was to analyze the performance of the aforementioned control techniques in terms of completion time, positioning precision, path length and required human energy so to demonstrate the effectiveness of the developed **VAF** over the traditional invariant control techniques. Before the start of the experiments, in order to increase the operator awareness of the robot motion, each volunteer tried to move the end-effector of the manipulator first with the **IAF-M** control technique. Then, when the subject got quite used and he/she felt more confident in handling the manipulator, the control technique was switched to the more reactive **IAF-L**. During this period of trials, the subject can lead the robot where he/she desires, without having any information about the operations that he/she will be asked to perform. As it can be noticed from Fig. 4.5, starting from the selected initial position the operator could not reach the target pose following a linear path because of the presence of the robot structure, being instead obliged to follow a certain curved path.

4.3.1 Outcomes

In this section the performance in terms of completion time, positioning precision, path length and required human energy obtained using the developed variable admittance control technique are compared with those of the invariant admittance control.

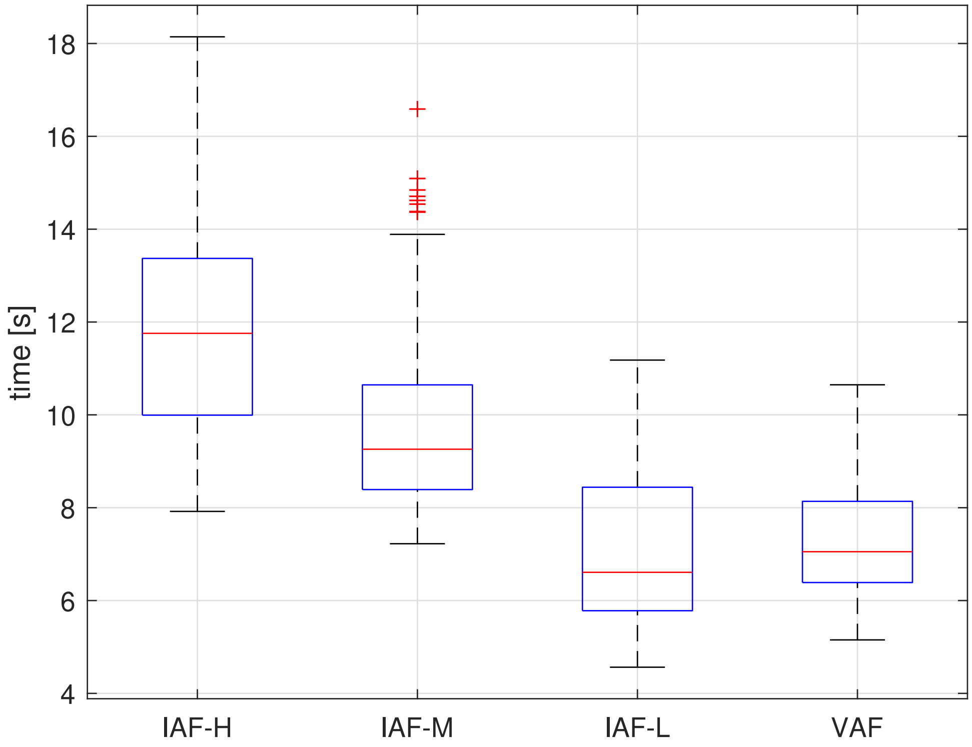

Figure 4.6: Statistics of the time needed to complete the path with the different control techniques.

As it is observable from Fig. 4.6, in order to complete the path with **VAF** it is only necessary a 5 % more time than **IAF-L**. However, the variability of the results is lower due to the ability of **VAF** to help the human operator in approaching the goal position. Moreover, **VAF** takes almost 30 % and 70 % less time of the **IAF-M** and **IAF-H** respectively.

A similar comparison can be done in terms of the human energy required to complete the path.

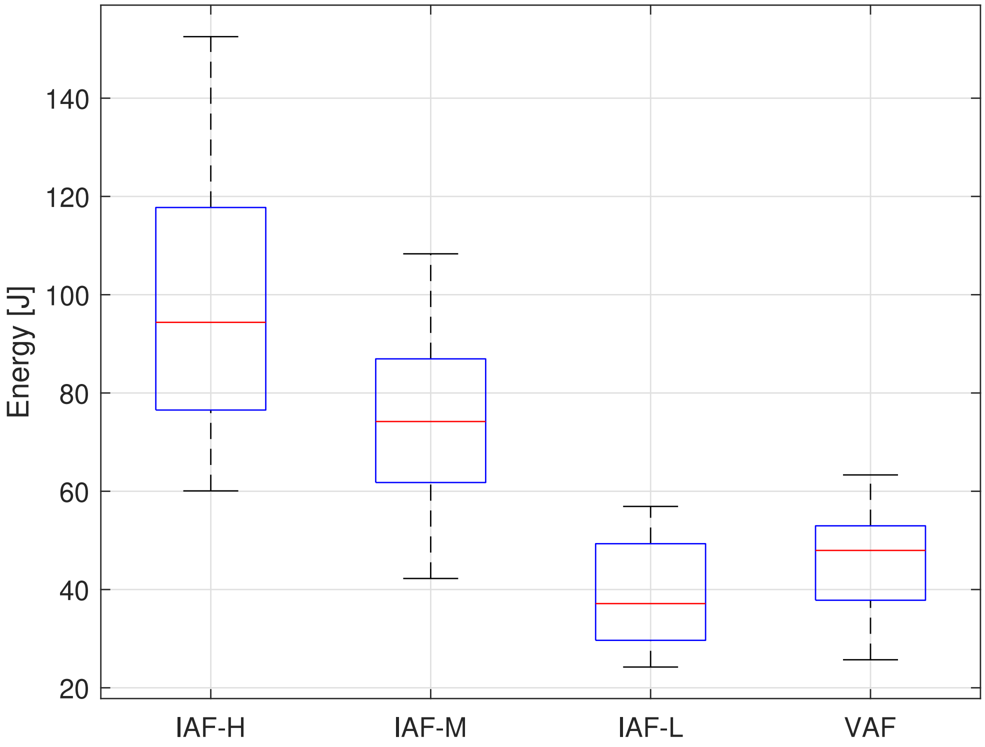

Figure 4.7: Statistics of the energy needed to complete the path with the different control techniques.

From Fig. 4.7 it is possible to understand that, from the fatigue relief point of view, the developed technique works quite well. Indeed, given that the **IAF-L** and the **IAF-H** are, respectively, the least and the most energy demanding control technique implementable to manage the physical interaction between humans and robots, **VAF** requires a small additional effort with respect to **IAF-L**, while it is much less energy demanding with respect to **IAF-M** and **IAF-H**.

In general, from the literature it is known that using a variable admittance control technique the requested energy would be comparable to the one obtained

fixing the admittance parameters to a value between the minimum and maximum allowed ones. Therefore, the fact that the **VAF** outcomes are less energy demanding with respect to the **IAF-M** ones is a satisfactory result.
In Fig. 4.8 the positioning error performance is shown. Even though the results are quite similar and good (less than 1 cm in average) for the different techniques, **VAF** guarantees a higher precision than **IAF-L** and an almost equal one to **IAF-M**.

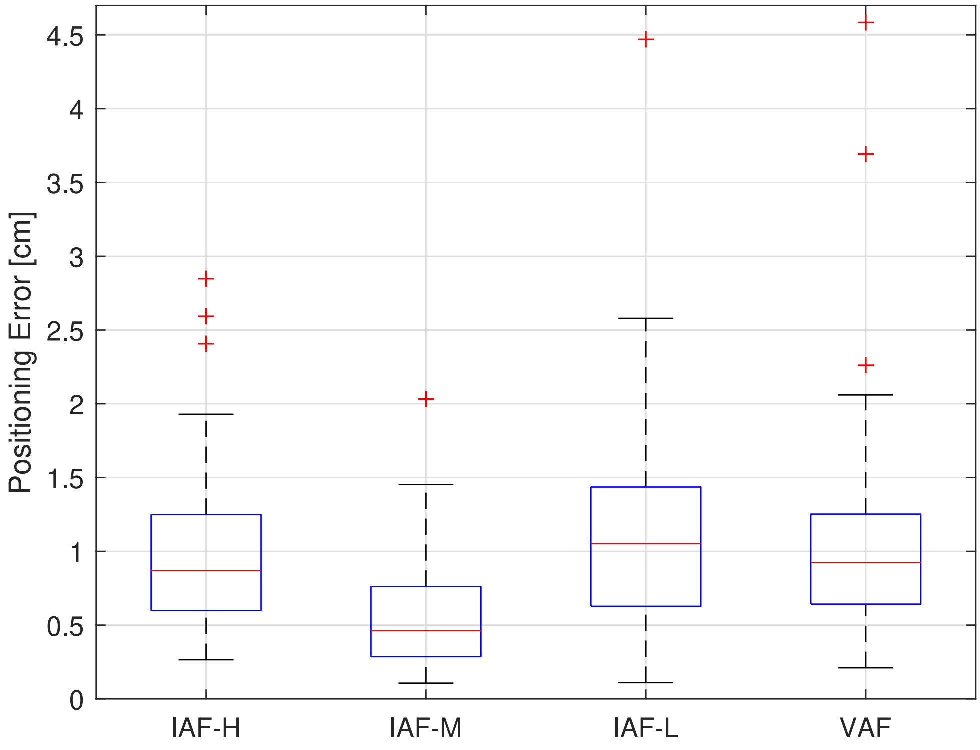

Figure 4.8: Statistics of the positioning precision with the different control techniques.

In Fig. 4.9 the statistics of the path length obtained with the different techniques is depicted. From these statistical results it is possible to observe that the **VAF** allows the human to complete the task along a shorter path than with all the other techniques, thanks to its ability of redirecting the him/her towards the goal.

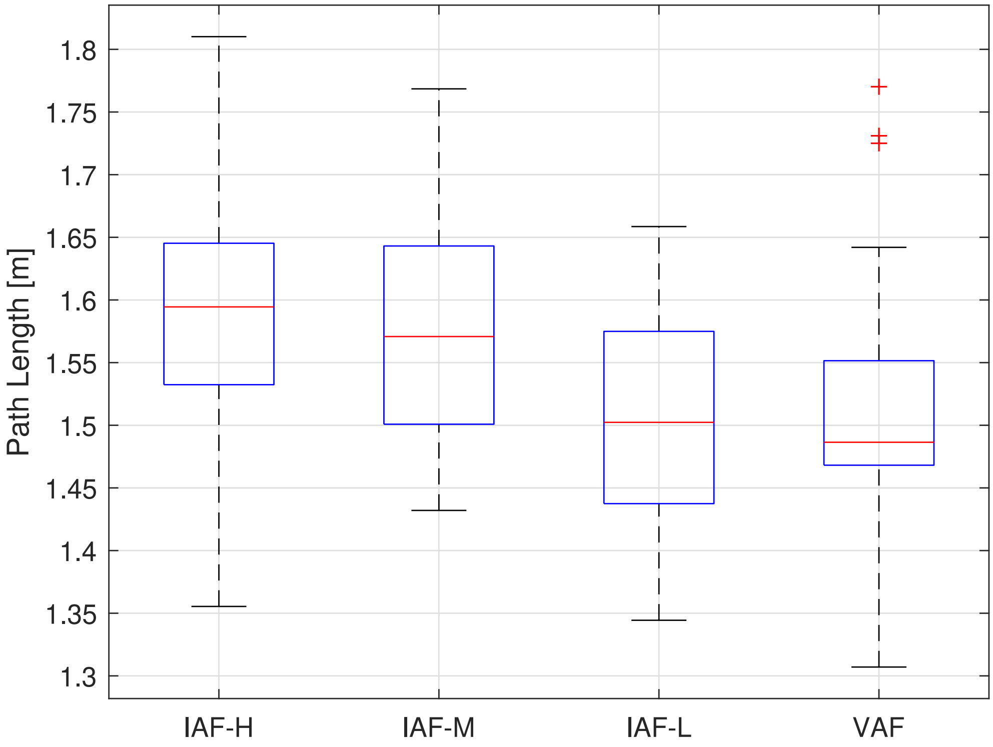

Figure 4.9: Statistics of the path length with the different control techniques.

Another interesting feature that emerges looking at the performance of **IAF** techniques is that the higher the inertia (proportional to the damping), the longer the path. This occurs because the speed direction of a moving object is difficult to be changed if its inertia is increasing. This justifies the need of the **VAF** to help the human in redirecting towards the desired target.

In Fig. 4.10, the behavior of the damping parameter of all the analyzed techniques with respect to a normalized time scale is reported, while Fig. 4.11 is an enlargement of its final part. The damping parameter of the **IAF-L**, **IAF-M**, **IAM-H** are represented with the green, magenta and red solid lines respectively, while its mean value for the **VAF** is depicted with the blue solid line. The dashed blue lines indicate the 75th and 25th percentile of VAF damping.

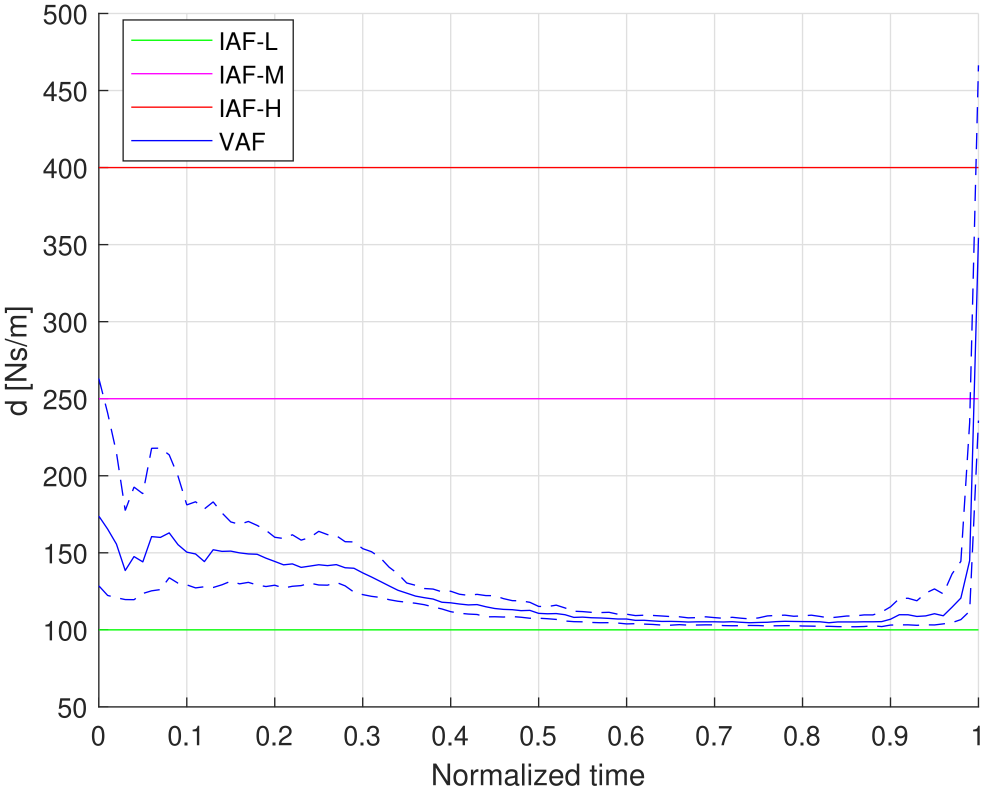

Figure 4.10: Behaviour of the virtual damping in a normalised time scale for the IAF-L, IAF-M, IAF-H and VAF with its 75th and 25th percentile.

An interesting thing to be noticed from figure 4.10 is that, with the **VAF**, the human is guiding the robot straight towards the path just after the 30% of the trajectory time. This can be understood observing that, after the first 30% of time, the damping takes the minimum value, meaning that the human is moving straight to the target.

Moreover, because of the presence of the robot, at the beginning of the path the operator cannot go straight and therefore the damping of **VAF** cannot be at the minimum value. After the 30% of the time, the damping starts to settle at the minimum value and also the corresponding percentiles define a smaller bandwidth around its mean value. Then, the **VAF** damping remains at its minimum value for a 55% of the total time until the end of the path, when the human has to brake in correspondence of the goal. Indeed in this latter phase, as it can be seen from Fig. 4.11, the **VAF** mean value almost reaches the maximum damping.

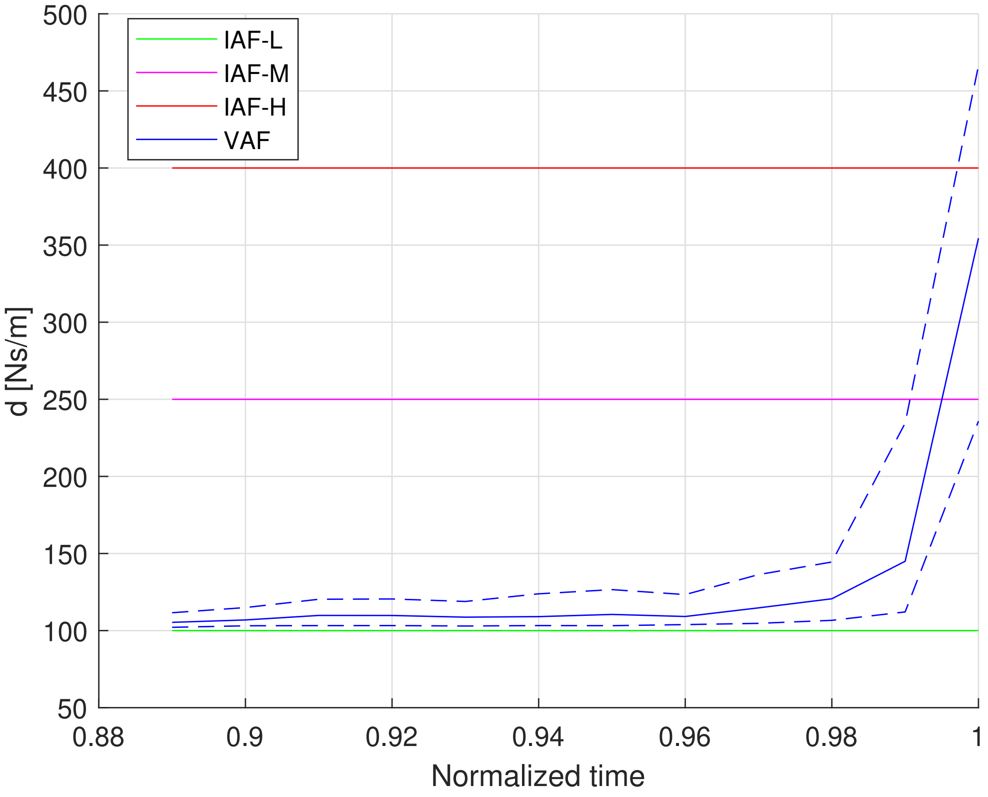

Figure 4.11: Zoom of the behaviour of the virtual damping in a normalised time scale for the IAF-L, IAF-M, IAF-H and VAF with its 75th and 25th percentile.

After this set of experiments, all the volunteers were asked to answer two questions in order to compare the experienced feelings when using the four different techniques. In particular, they were asked to give a mark (from 1 to 10) to the experienced effort and to the ease of approach to the predefined goal.

Fig. 4.12 shows the relative results between the **VAF** and the **IAF** techniques in terms of perceived effort, while Fig. 4.13 reports the relative results between the **VAF** and the **IAF** techniques in terms ease of approaching the target. As it can be observed, the **VAF** requires less than 20% additional effort with respect to **IAF-L**, and it is more than 20% easier then the **IAF-L** in approaching the goal. At the same time, the **VAF** requires 80% and 50% less energy than **IAF-H** and **IAF-M** respectively. Moreover, **VAF** results can be considered less precise by 40% and 30% than **IAF-H** and **IAF-M** respectively. Therefore, it is possible to conclude that, also from the operators subjective point of view, **VAF** is globally better than the **IAF-H** and **IAF-M**.

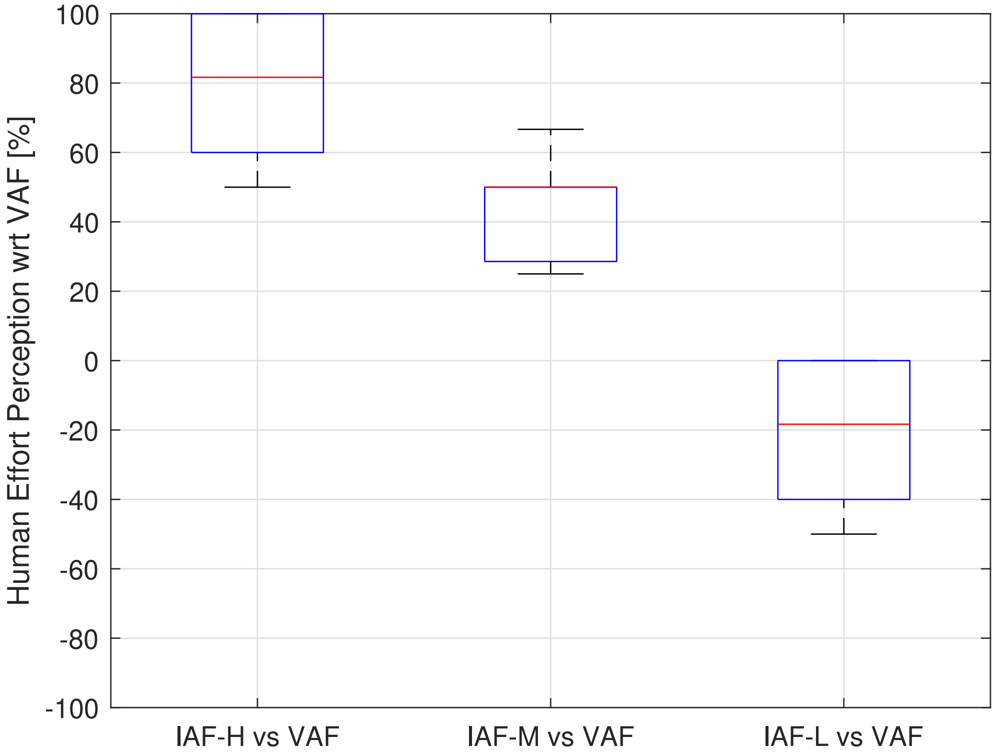

Figure 4.12: Questionnaire statistics of the effort perceived by the operators when using the invariant control techniques compared with the one perceived when using the variable strategy. The relative results are expressed in percentage.

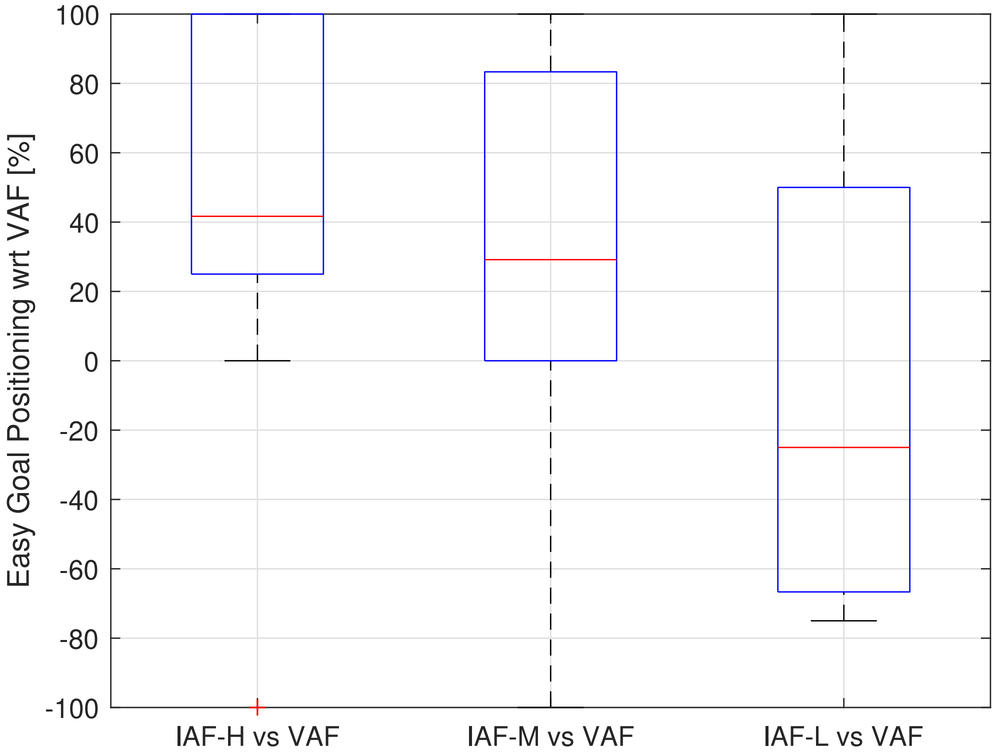

Figure 4.13: Questionnaire statistics of the easy of approaching the goal position of the invariant control techniques with respect to the variable strategy. The relative results are expressed in percentage.

4.4 Unknown goal experiment: objectives, set-up and results

The purpose of this set of experiments was to demonstrate the effectiveness of the proposed approach in returning to the worker a natural and intuitive directional feedback, which allows him/her to reach, with a certain level of precision, a goal that he/she cannot directly see (*e.g.* because of to the size of the transported load). During the accomplishment of this task, since the **IAF** techniques cannot distinguish among space directions, only the **VAF** proposed technique was applied.

Each volunteer was asked to move the robot from its usual starting pose to three different unknown targets, whose position was randomly selected within the robot operating space. During this operation, the human had only 40 seconds and just one shot to approach each goal position, as accurately as possible. For this type of test, since the operator did not have to know where the position of the target was, the laser previously mounted on the tip of the handle was switched off and the goal was not marked on the floor. If the operator had reached what he believed to be the target before the time was elapsed, he would have to stop the movement of the end-effector anyway. At the end of this set of experiments, the volunteers were still asked to answer four questions in order to evaluate their experience, assigning to each of them a mark from 1 to 10.

In the following, the topic of each question is described:

- **Q1**: the ease of perception of guiding the robot towards the right direction;
- **Q2**: the possibility of improving the performance with more practise;
- **Q3**: the clarity with which they perceived to be in proximity of the target;
- **Q4**: the confidence in having reached the unknown goal position with a good precision.

4.4.1 Outcomes

The statistics concerning the final position reached by the operator at the end of the aforementioned task are reported in Fig. 4.14 for each of the three unknown goals. Even though the volunteers had never tried such a task before and had no experience of a physical interaction with a robot, the obtained results are very satisfactory.

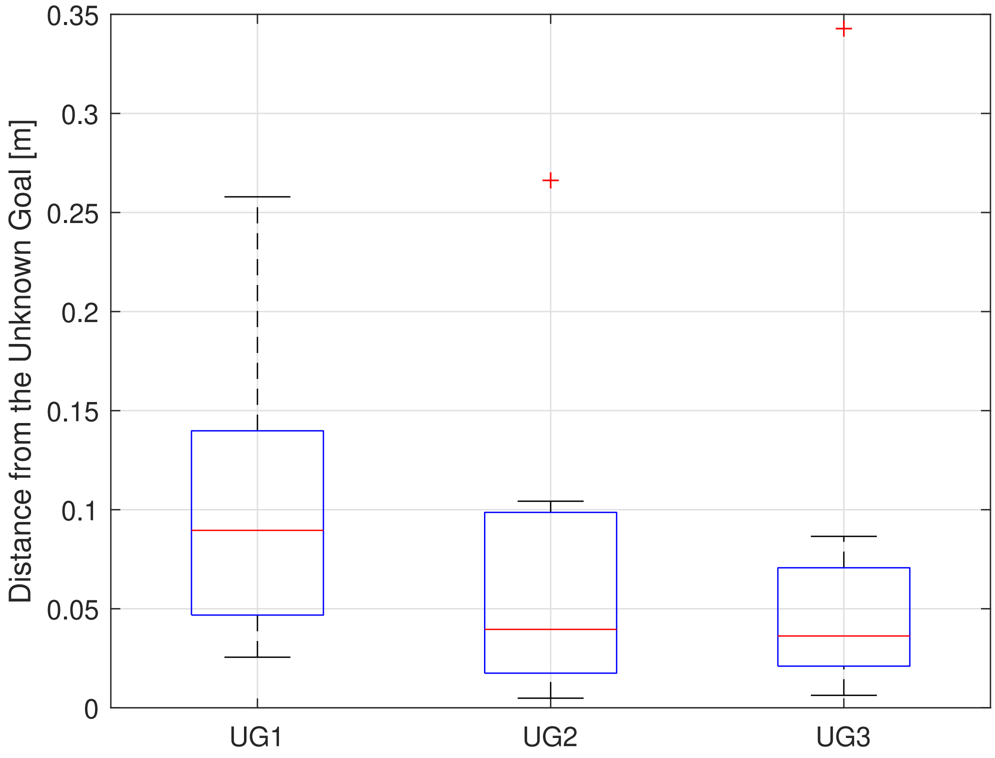

Figure 4.14: Statistics of the positioning precision in reaching the subsequent unknown random goal position.

Indeed, from Fig. 4.14, it is possible to observe that, with the first trial, the mean error is already under 10 cm and with the third one it is under 4 cm, with low variability. Thus, the importance of experience and practise can be clearly inferred just looking at the performances improvements in terms of positioning accuracy. Indeed, when passing from the first to the third unknown goal, both the mean value and the difference between the minimum and maximum distance from the target was reduced.

From the analysis of the evaluation test compiled by each subject, the results shown in Fig. 4.15 were obtained.

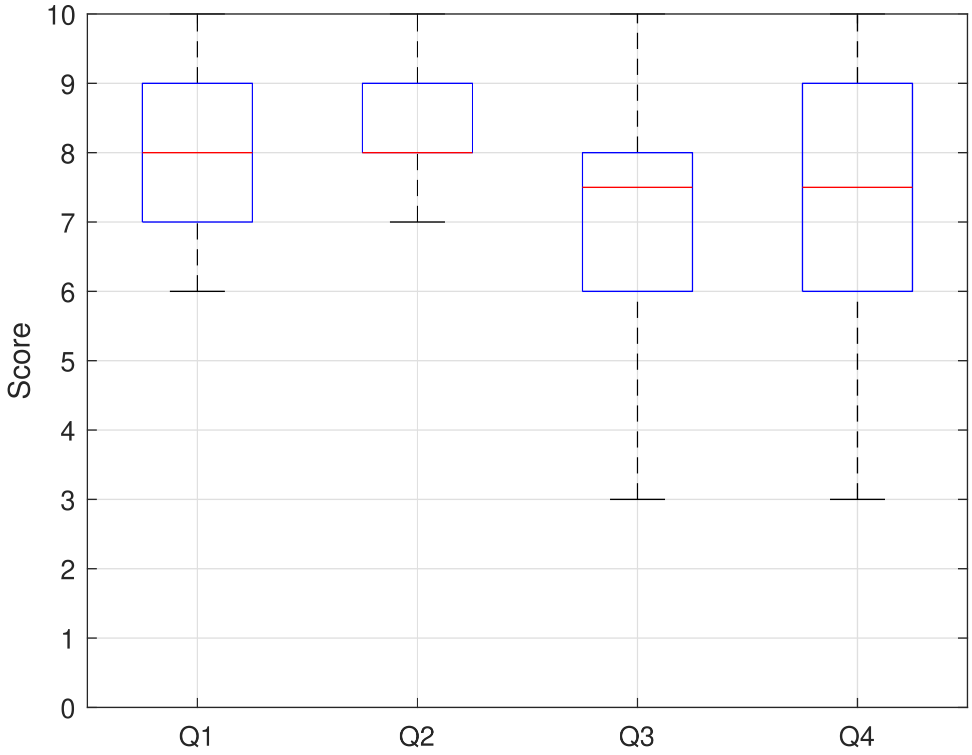

Figure 4.15: Questionnaire statistics about the unknown goal approaching experience.

The volunteers argued that it was easy to perceive the right direction of motion and that, with some additional practise, the performance would surely increase. Moreover, they state that they clearly understood of being near to the goal position and therefore they were confident of reaching the target with a good accuracy.

Chapter 5

Conclusions

In the present work, a new extended physical interpretation of the classical admittance control for human-robot physical interaction in manual guidance applications is proposed.

In general, the variable admittance control techniques aim at making the virtual parameters of the admittance filters change as a function, for example, of the intensity of the force applied by the human or of the end-effector velocity and/or acceleration norm. However, less attention has been paid to the variation of the virtual parameters in dependence of the direction of the applied force and the target position. Hence, the main contribution of the present work is to enrich the classical algorithms with the ability to help the human in directing towards a predefined goal position. The developed strategy is based on a geometrical interpretation of the admittance control techniques. On the one hand, when a fixed admittance control is taken into account, the virtual parameters can be modelled as the radius of a sphere centered in the origin of the local frame. On the other hand, when a variable admittance control is considered, the radius of the sphere has to change in accordance to the intensity of the applied force, velocity and/or acceleration of the end-effector.

In order to modulate the virtual parameters of the admittance filter, accounting for the relative direction of the applied force with respect to the goal position, an alternative geometrical 3-dimensional shape, namely an ellipsoid, is adopted. It is centered at the origin of the local frame and both the direction and the length of its three semi-axes are fundamental for the development of the algorithm. The direction of the first axis, which represents the *minimum effort* one, is selected through a minimum curvature path: it corresponds to the line connecting the actual position of the end-effector with a point belonging to the path, which in turn is selected exploiting an exponential expression. This allows the operator to be less assisted at the beginning of the motion and more assisted when approaching the target position. Its length, for what concerns the damping ellipsoid, is set equal to the minimum damping value, while the length of the other two semi-axes is set equal to the maximum damping. Indeed, the virtual parameters are computed as the distance between the centre of the ellipsoid and the point of intersection of the ellipsoid surface with a line directed as the human force. In this way, if the force is directed as the first principal axis, the damping value will be set at its minimum, so that the human operator perceives a lower resistance when moving towards this direction. Otherwise, it is increased up to its maximum, making the operator experience a higher effort.

Referring to the inertia ellipsoid, it is oriented as the damping one and the length of its semi-axes is assigned to make the bandwidth of the admittance filter constant during the execution of the task, allowing for a more intuitive interaction for the human operator.

Moreover, since according to the literature a low damping is advisable when the human is pushing towards the target, while high damping is convenient when braking in proximity of it, the virtual damping ellipsoid is reshaped, dividing it into two halves with a plane defined by its second and third axes and normal to the direction of the first axis. The half belonging to the half-space containing the target is the same of the previous ellipsoid; the length of the first semi-axis of the other half can be set either greater or equal to the maximum length of the other

two, while its orientation is still the same of the previous one.
The performance of the proposed controller are evaluated by means of point to point cooperative motions with 10 volunteers and compared in terms of human energy, completion time, positioning error, and path length with low (IAF-L), medium (IAF-M) and high (IAF-H) parameters constant damping controllers. The results show that the proposed strategy is the best compromise between the constant low damping and constant high damping control strategies. Indeed, the obtained statistics show that it requires a small additional effort with respect to IAF-L, while it is much less energy demanding with respect to IAF-H. At the same time, from the positioning precision point of view, it allows a higher precision than IAF-L, while an almost equal one to IAF-M. Eventually, the ability of approaching completely unknown goals is tested and successfully validated. In this case, the statistics show that the operator can reach an unknown target with a good level of precision, *i.e.* a maximum positioning error below 10 cm and a minimum one below 4 cm, thanks to the intuitive and natural feedback that this strategy returns to the human operator. As a consequence of these results, this algorithm might be applied even in case the operator's view is obstructed by the bulky dimensions of the transported object.

5.1 Future developments

Since the obtained results are satisfactory, some hints on possible improvements can be proposed for future studies and applications.

- The developed algorithm was structured thinking of its application on manipulators characterized by huge outreach, but it was tested on the IRB 140 which is quite limited from this point of view. For this reason, it might be interesting to understand the real potentialities of the developed method with this type of manipulators.

- The developed technique might be merged with those existing in literature. Then, one could conceive of varying the length of the semi-axis of the ellipsoid according to the module of the force applied by the human or the speed of movement, together with the acceleration of the end-effector.

- The algorithm has been tested taking into account the presence of a single target. A possible improvement could be its application when different possible goals are placed in the work space. In this situation, first of all, it would be desirable to leave the operator quite free to choose the end-effector direction of motion, making him/her feel a low level of resistance in any direction. Then, setting probabilistic thresholds, it would be possible to identify the target the operator is heading to and, consequently, select the direction of minimum effort, which corresponds to the one of the first principal axis.

- Another interesting feature to be evaluated might be the effectiveness of the applied algorithm in case of the existence of a target orientation of the end-effector. In the frame of the present work, the handle mounted on the end-effector was fixed to prevent its rotations, even in case of torque application. Hence, changing the handle type and extending the algorithm to the rotational movements, the capability of the operator to orient the handle as prescribed just following his/her feeling could be studied.

Bibliography

[1] Irb 140 - industrial robot. `https://new.abb.com/products/robotics/it/robot-industriali/irb-140`.

[2] Seven common application for cobots. `https://www.machinedesign.com/mechanical-motion-systems/article/21836350/7-common-applications-for-cobots`.

[3] L. Bascetta, G. Ferretti, G. Magnani, and P. Rocco. Walk-through programming for robotic manipulators based on admittance control. *Robotica*, 31(7):1143–1153, 2013.

[4] J. E. Colgate, J. Edward, M. A. Peshkin, and W. Wannasuphoprasit. Cobots: Robots for collaboration with human operators. *International Mechanical Engineering Congress and Exposition, Atlanta*, pages 433–440, 1996.

[5] F. Dimeas and N. Aspragathos. Fuzzy learning variable admittance control for human-robot cooperation. *2014 IEEE/RSJ International Conference on Intelligent Robots and Systems*, pages 4770–4775, 2014.

[6] F. Dimeas and N. Aspragathos. Reinforcement learning of variable admittance control for human-robot co-manipulation. *2015 IEEE/RSJ International Conference on Intelligent Robots and Systems (IROS)*, pages 1011–1016, 2015.

[7] F. Dimeas and N. Aspragathos. Online stability in human-robot cooperation with admittance control. *IEEE Transactions on Haptics*, 9(2):267–278, 2016.

[8] V. Duchaine and C. M. Gosselin. General model of human-robot cooperation using a novel velocity based variable impedance control. *Second Joint EuroHaptics Conference and Symposium on Haptic Interfaces for Virtual Environment and Teleoperator Systems (WHC'07)*, pages 446–451, 2007.

[9] V. Duchaine, B. Mayer St-Onge, D. Gao, and C. Gosselin. Stable and intuitive control of an intelligent assist device. *IEEE Transactions on Haptics*, 5(2):148–159, 2012.

[10] B. Siciliano et al. *"Modellistica, Pianificazione e Controllo"*. The McGraw-Hill, 2008.

[11] F. Ferraguti, R. Villa, C. Talignani Landi, A. M. Zanchettin, P. Rocco, and C. Secchi. A unified architecture for physical and ergonomic human–robot collaboration. *Robotica, Cambridge University Press*, 38(4):669–683, 2020.

[12] F. Ficuciello, L. Villani, and B. Siciliano. Variable impedance control of redundant manipulators for intuitive human–robot physical interaction. *IEEE Transactions on Robotics*, 31(4):850–863, 2015.

[13] J. Fryman and B. Matthias. Safety of industrial robots: From conventional to collaborative applications. *ROBOTIK 2012; 7th German Conference on Robotics*, pages 1–5, 2012.

[14] G. Hoffman and C. Breazeal. Effects of anticipatory action on human-robot teamwork efficiency, fluency, and perception of team. *Proceedings of the ACM/IEEE International Conference on Human-Robot Interaction*, page 1–8, 2007.

[15] N. Hogan. Impedance control: An approach to manipulation. *American Control Conference*, pages 304–313, 1984.

[16] R. Ikeura and H. Inooka. Variable impedance control of a robot for cooperation with a human. *Proceedings of 1995 IEEE International Conference on Robotics and Automation*, 3:3097–3102 vol.3, 1995.

[17] R. Ikeura, T. Moriguchi, and K. Mizutani. Optimal variable impedance control for a robot and its application to lifting an object with a human. *Proceedings. 11th IEEE International Workshop on Robot and Human Interactive Communication*, pages 500–505, 2002.

[18] A. QL Keemink, H. Van der Kooij, and A. HA. Stienen. Admittance control for physical human–robot interaction. *The International Journal of Robotics Research*, 37(11):1421–1444, 2018.

[19] A. Lecours, B. Mayer-St-Onge, and C. Gosselin. Variable admittance control of a four-degree-of-freedom intelligent assist device. *2012 IEEE International Conference on Robotics and Automation*, pages 3903–3908, 2012.

[20] A. Sharkawy, P. N. Koustournpardis, and N. Aspragathos. Variable admittance control for human-robot collaboration based on online neural network training. *2018 IEEE/RSJ International Conference on Intelligent Robots and Systems (IROS)*, pages 1334–1339, 2018.

[21] C. Talignani Landi, F. Ferraguti, L. Sabattini, C. Secchi, and C. Fantuzzi. Admittance control parameter adaptation for physical human-robot interaction. *2017 IEEE International Conference on Robotics and Automation (ICRA)*, pages 2911–2916, 2017.

[22] T. Tsumugiwa, R. Yokogawa, and K. Hara. Variable impedance control with regard to working process for man-machine cooperation-work system. *Proceedings 2001 IEEE/RSJ International Conference on Intelligent Robots and Systems. Expanding the Societal Role of Robotics in the the Next Millennium (Cat. No.01CH37180)*, 3:1564–1569 vol.3, 2001.

[23] T. Tsumugiwa, R. Yokogawa, and K. Hara. Variable impedance control based on estimation of human arm stiffness for human-robot cooperative calligraphic task. *Proceedings 2002 IEEE International Conference on Robotics and Automation (Cat. No.02CH37292)*, 1:644–650 vol.1, 2002.

[24] R.Q. Van der Linde and P. Lammertse. Hapticmaster - a generic force controlled robot for human interaction. *Industrial Robot: An International Journal*, 30(6):515–524, 2003.

[25] A. M. Zanchettin and P. Rocco. Probabilistic inference of human arm reaching target for effective human-robot collaboration. *IEEE/RSJ International Conference on Intelligent Robots and Systems (IROS)*, pages 6595–6600, 2017.